Structural Optimization of Chinese Energy-Saving Solar Greenhouses and Ideal Canopy Design for Tomato Cultivation

Reporter: Yue Zhang

Date: Dec 5, 2024

12th GroIMP User and Developer Workshop

Contents

1 Introduction

Energy-saving solar greenhouses (ESG) are widely used the northern regions of China. However, challenges remain for high-quality winter production of heat-loving crops like tomatoes.

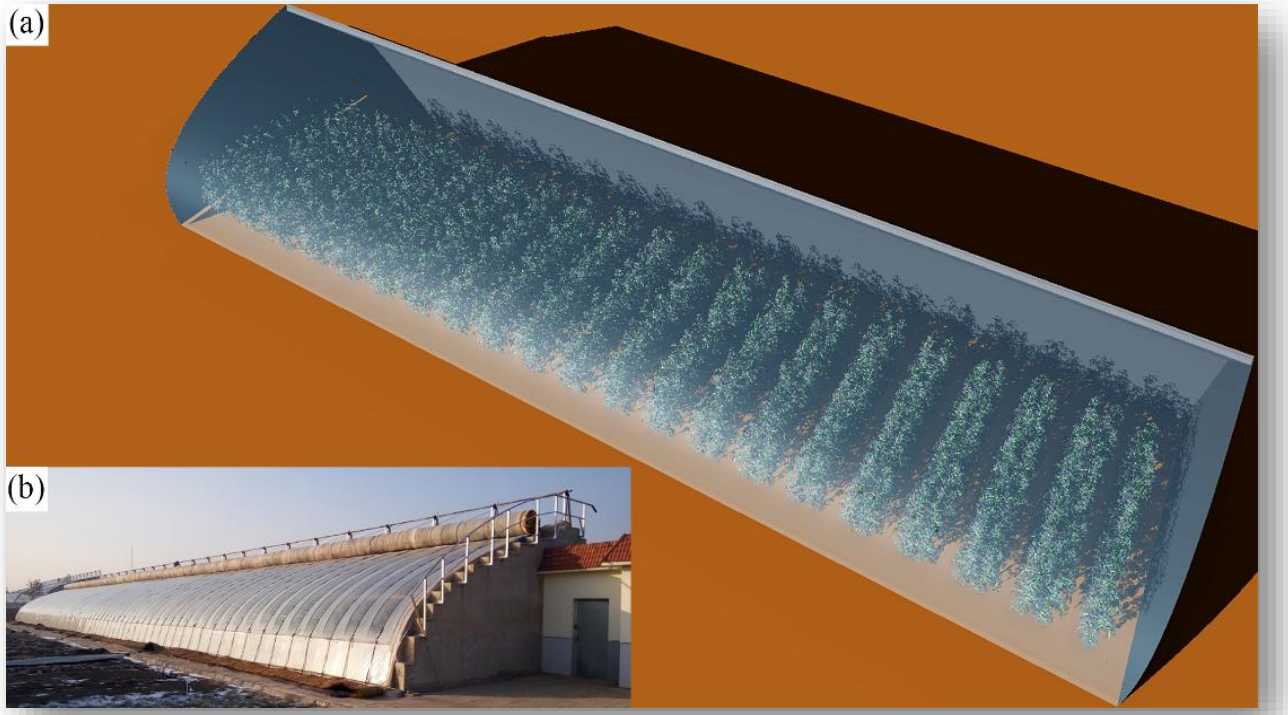

Photograph of the Liaoshen-type ESG (a), and the Virtual Solar Greenhouse along with the Tomatoes Cultivated Inside (b).

- **Inconsistent product quality**
- **Mechanized cultivation**
- **Automated cultivation**
- **Precision-controlled cultivation**

1 Introduction

To optimize the light environment in ESG, research must focus on two key aspects:

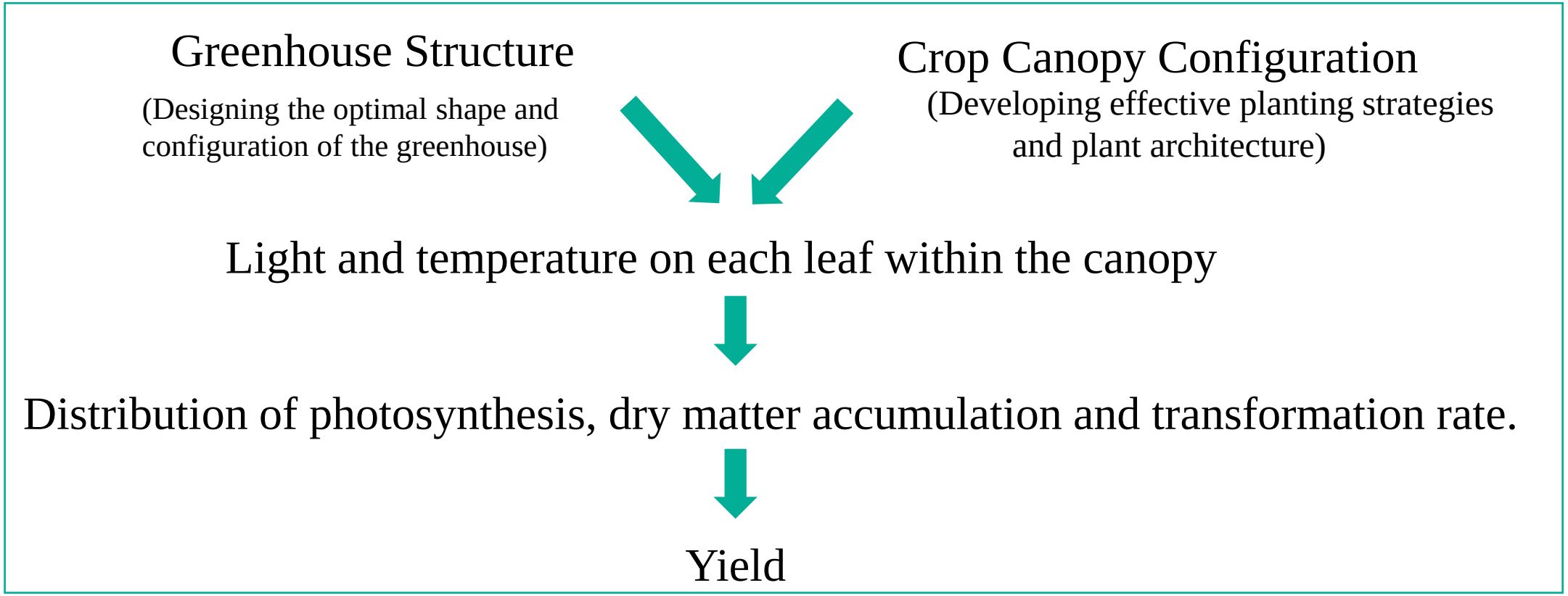

Contents

2.1 Collection of Structural and Physical Parameters of the Experimental Greenhouse and Tomatoes

- **Determination of Microenvironment and Architectural Parameters of the Second-generation Energy-saving Solar Greenhouses**
- **Determination of Morphological and Physical Parameters of Tomatoes**

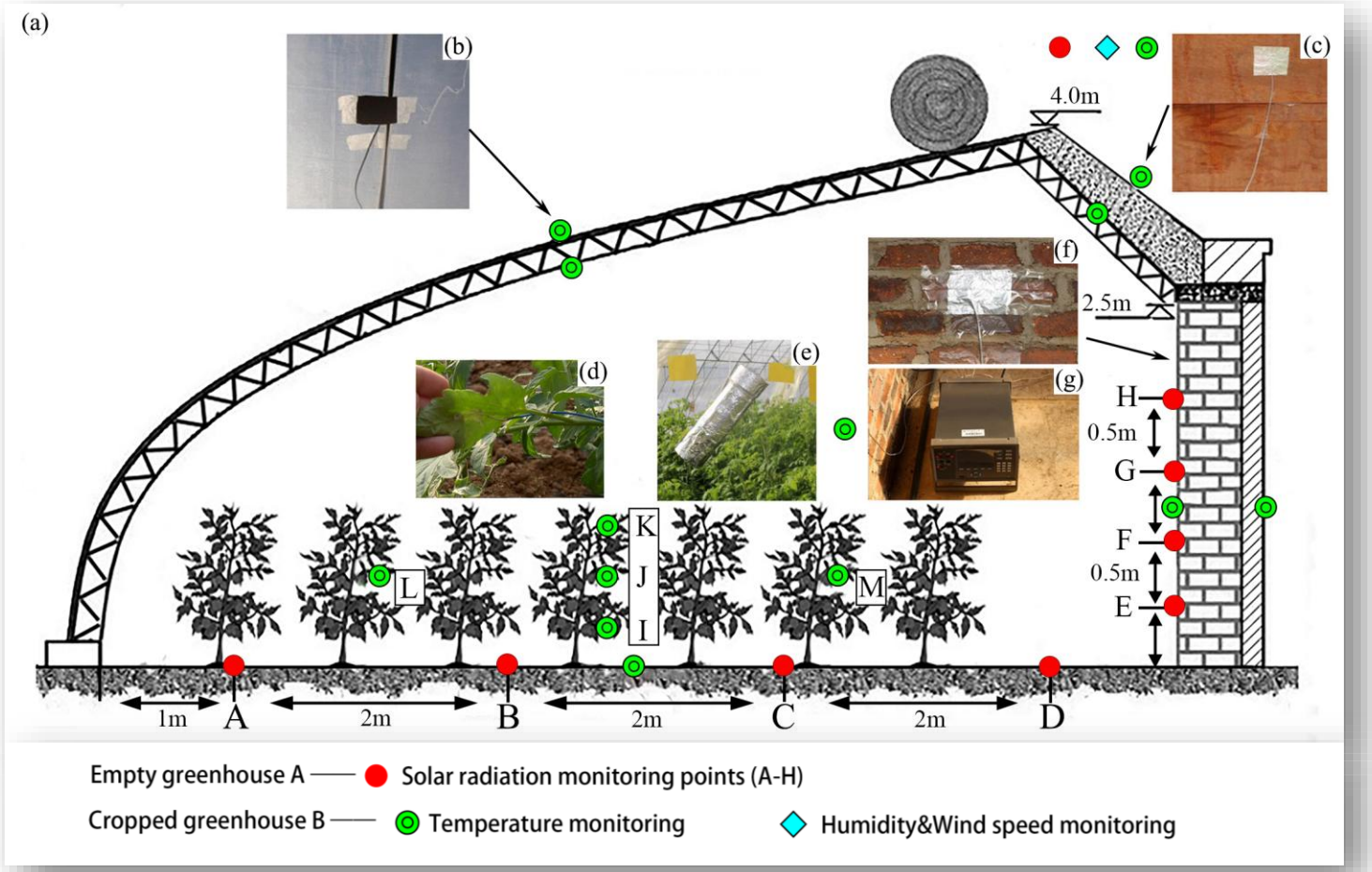

Schematic Diagram of the Positions of All Monitoring Points in the Empty Greenhouse (A) and the Greenhouse with Tomato Cultivation (B).

2.2 Light Environment Simulation Modeling

- **Establish a virtual light scene, a simulation model of the solar greenhouse, and virtual tomato crops using GroIMP platform.**

Photograph of the 3D model of a 30 m-long LSG, including the tomato canopy, with 41 rows, 13 plants in each row, totaling 533 plants, and a total of 113,529 tomato leaflets.

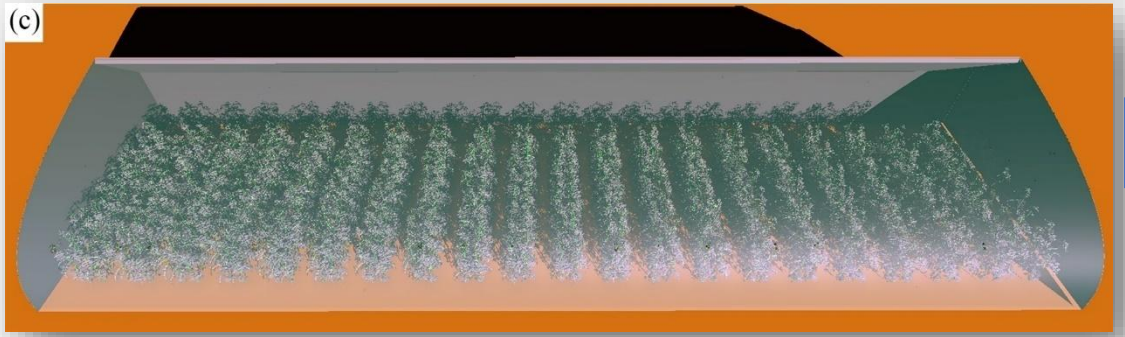

Visualization of the Solar and Sky Models (a): Snapshot of the 30×8×4-meter virtual greenhouse model (b).

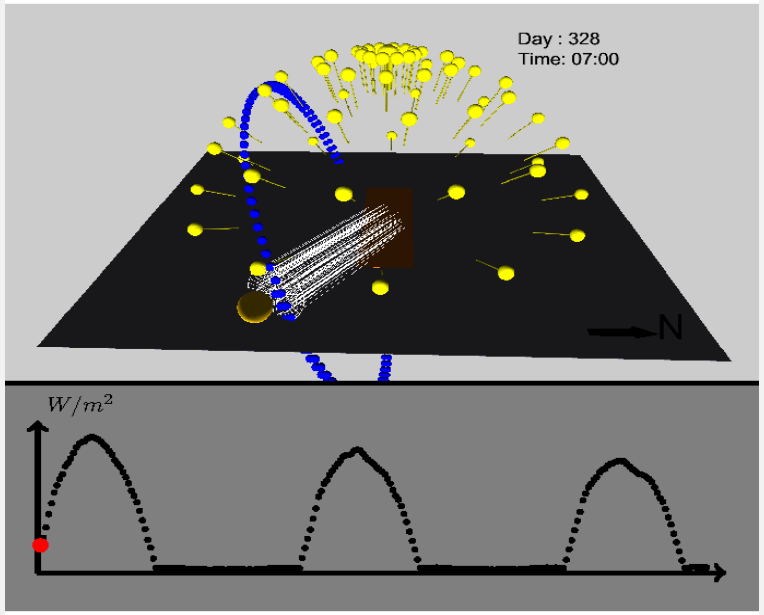

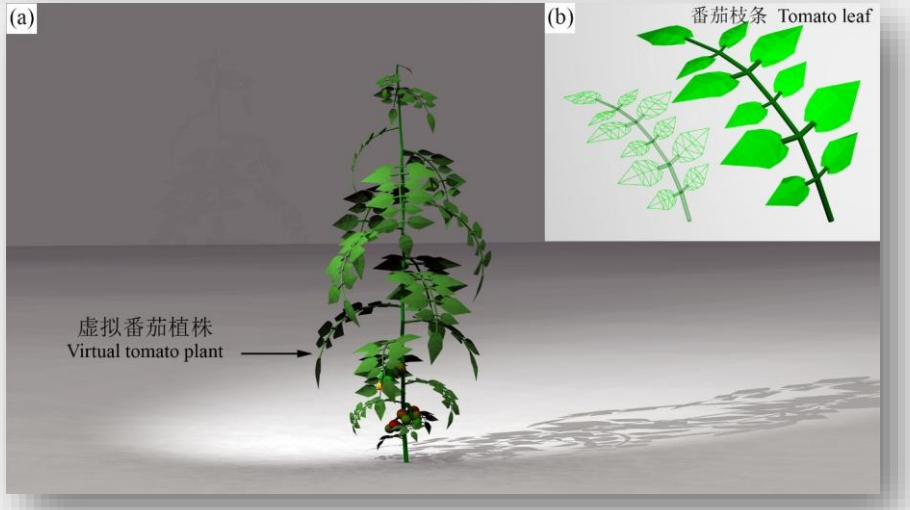

Rendered Image of a Single Adult Tomato Plant Used in the Tomato Canopy (a); Detailed Magnification of a Single Leaf and Wireframe Visualization of the Underlying Triangular Mesh Structure of the Leaflets (b).

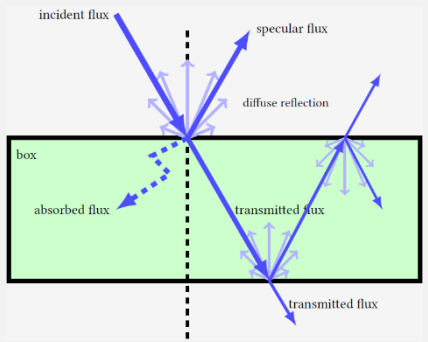

Motion Tracking Trajectory of Each Light Ray.

2.2 Light Environment Simulation Modeling.

- **Verification of Light Distribution on the Surfaces of Each Component Inside the Solar Greenhouse.**

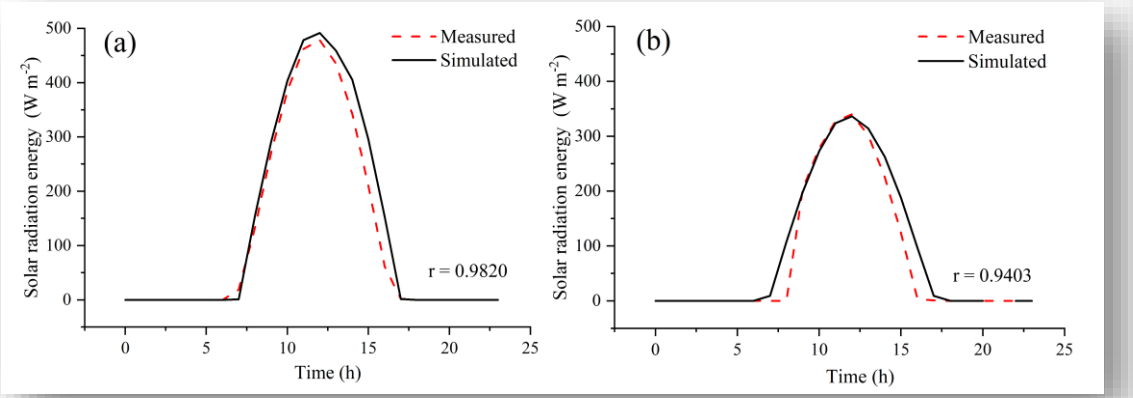

Average simulated radiation and measured radiation outdoors (a) and inside the greenhouse (b) during the daytime: 17th Nov, 2014.

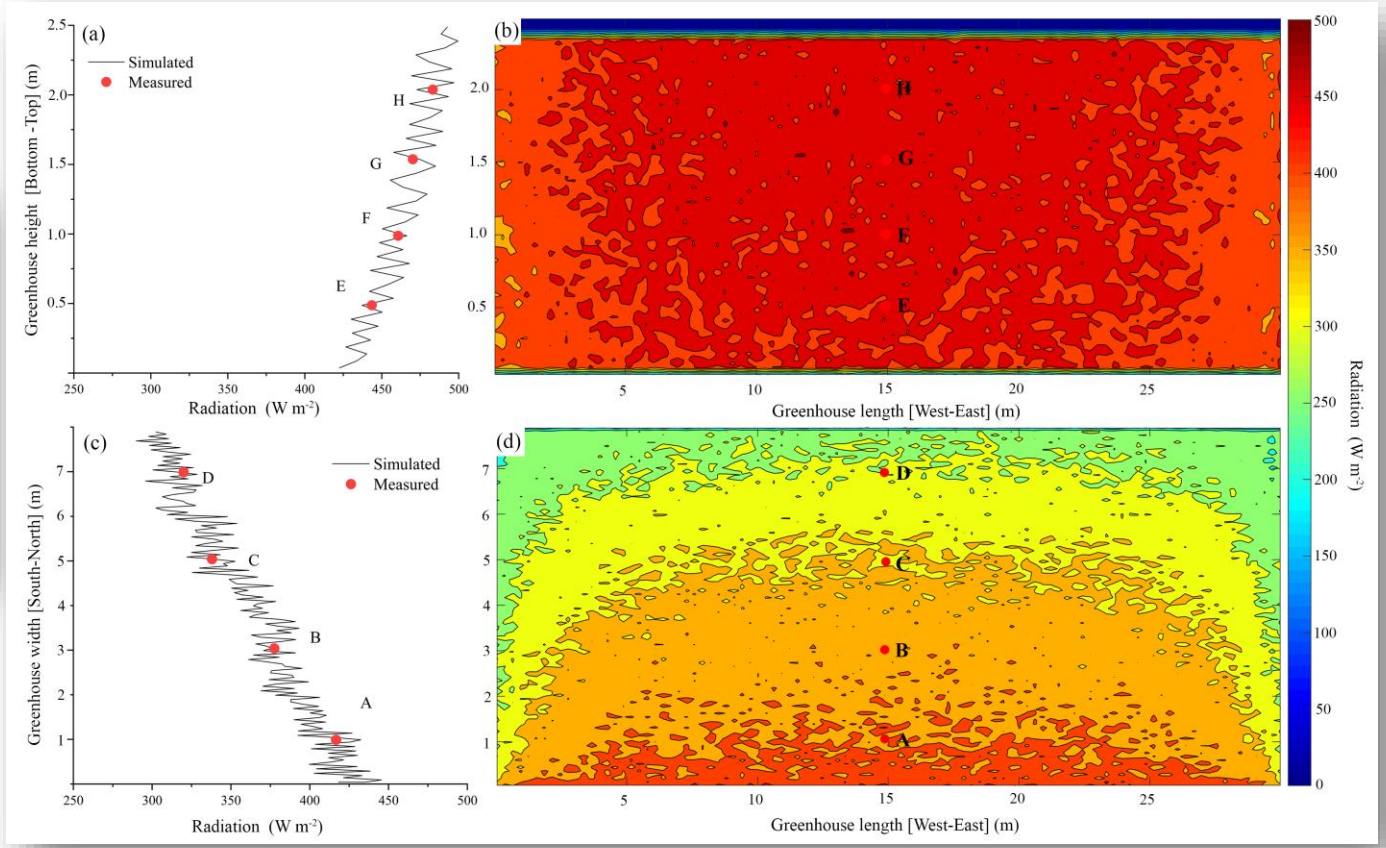

Distribution of solar radiation energy inside the unheated greenhouse at 12 noon for the north wall (Figures (a), (b)) and the ground (Figures (c), (d)) between the simulated values and the measured values.

2.2 Light Environment Simulation Modeling.

- **Establishment, Solution of the Energy Balance Equations for Each Part of the Greenhouse and Model Verification.**

The nonlinear differential equations containing 12 unknowns.

$T_a, T_c, T_w, T_{w1}, T_{wo}, T_r, T_{r1}, T_{ro}, T_s, T_{s1}, T_{s2}, T_c$

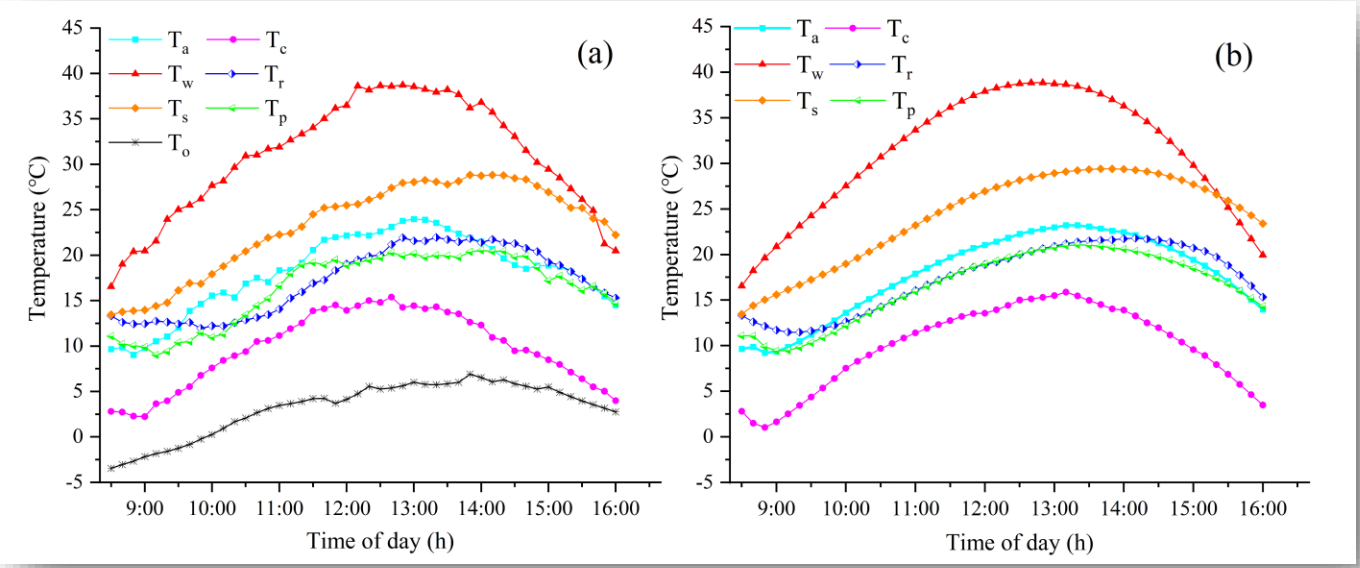

Measured values (a) and simulated values (b) of the average temperatures of the internal air, front roof, north wall, roof, soil, tomato canopy surface and environment on a typical winter day (17-11-2014).

RMSE (Root Mean Square Error) of temperature prediction and the correlation coefficient r between simulation and measurement.

	T_a	T_c	T_w	T_r	T_s	T_p
RMSE	1.0179	1.0002	0.8567	0.9398	1.0704	0.7634
r	0.9528	0.9576	0.9671	0.9425	0.9218	0.9025

Verification of Temperature Distribution in Solar Greenhouses and Tomato Populations

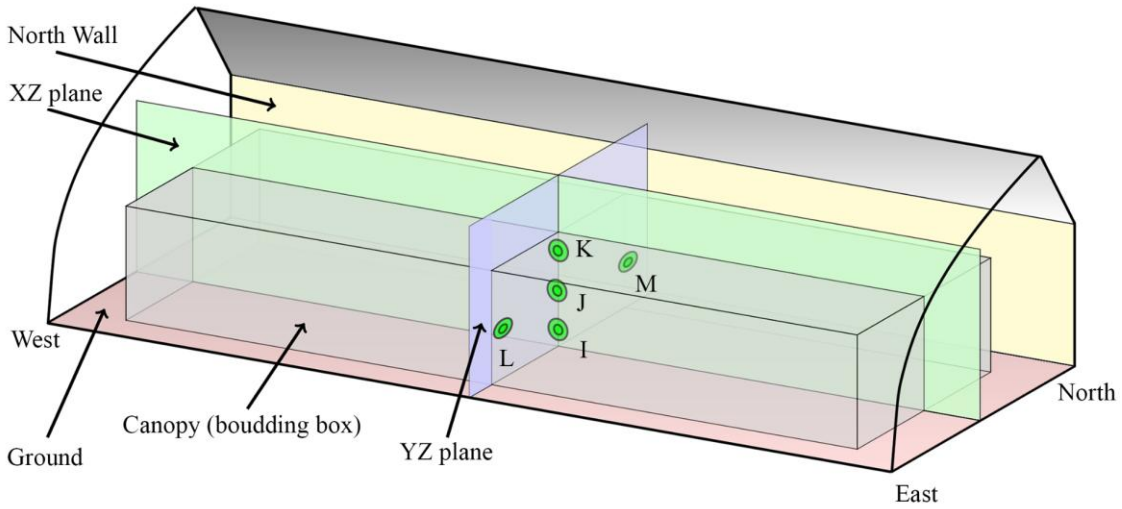

Schematic plot of the greenhouse, showing the positions of all discussed planes, cross sections (XZ plane and YZ plane), and the plant canopy. Highlighted as green dots and labelled with I-M are the locations of the reference points where the temperature was measured within the plant canopy.

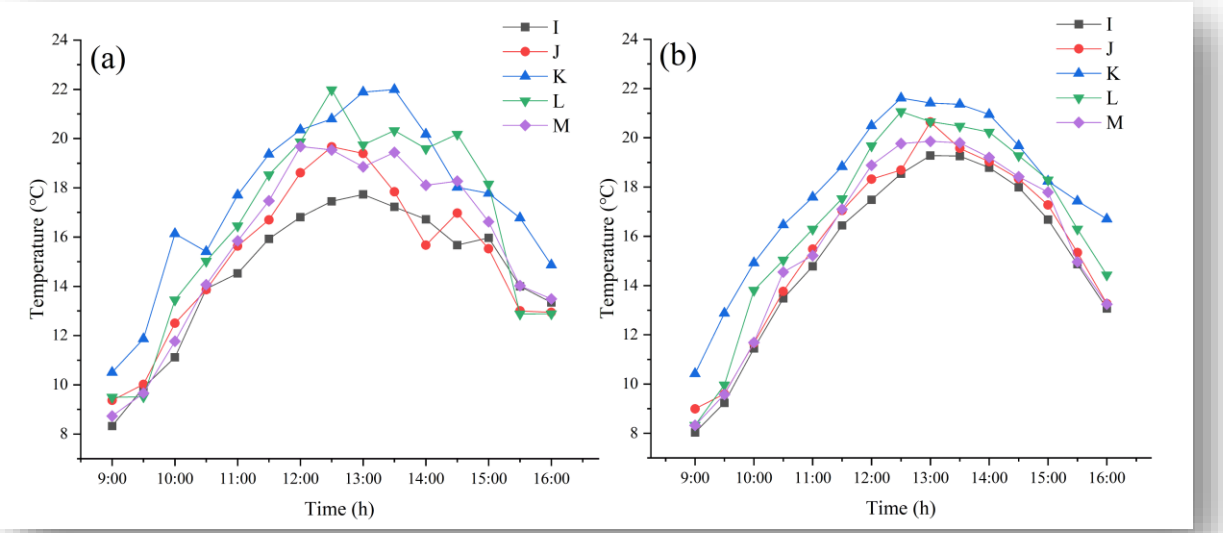

Data points of measured (a) and simulated (b) canopy temperature values, as shown in Figure 2, I-K (XZ plane) and L-M (YZ plane), on a typical winter day (17-11-2014) in the planting greenhouse. The relatively low values shown in some of the measured on-site data might be due to certain deviations caused by environmental factors such as wind, plant movement, or the shadow of the front roof structure.

RMSE (Root Mean Square Error) of canopy temperature point prediction and the correlation coefficient r between simulation and experiment.

	I	J	K	L	M
RMSE	1.1629	1.3791	1.1437	1.1489	0.6474
r	0.9665	0.8809	0.8983	0.9116	0.9730

Temperature Distribution in Solar Greenhouses and Tomato Populations

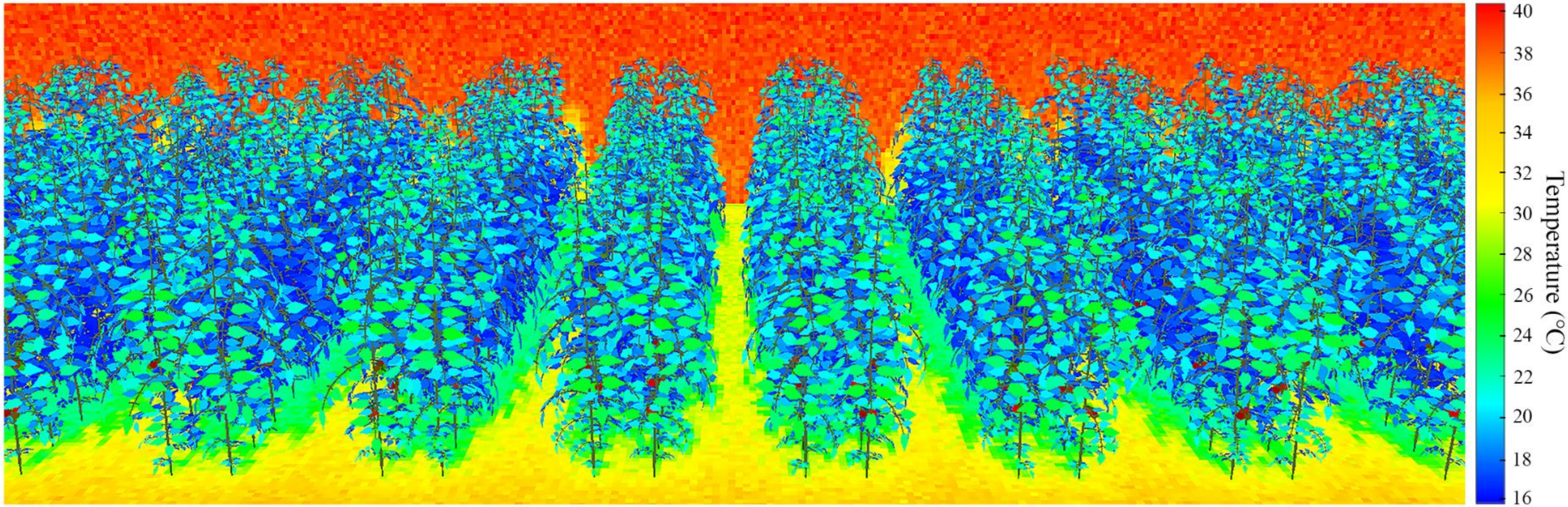

The thermographic image simulated within the LSG 3D model at 12 noon on a typical winter day (17-11-2014).

2.4 Simulation of Photosynthetic Rate

Simulation of the Photosynthetic Rate of Tomato Leaves in Solar Greenhouses.

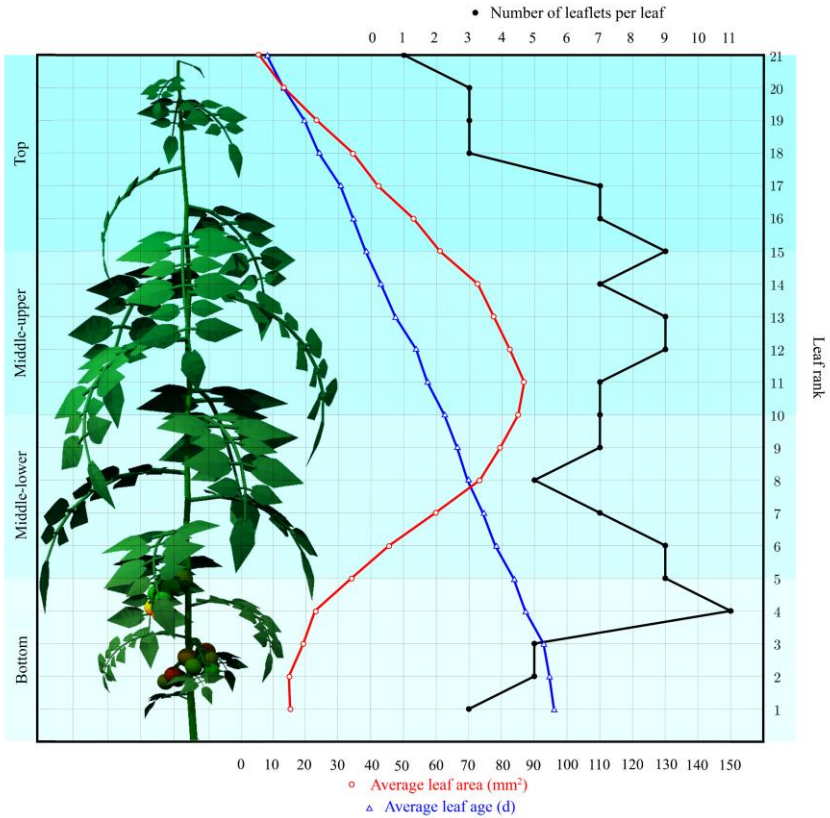

Images of simulated individual adult tomato plants used in the 3D canopy model, including leaf grading: top (levels 15 - 21), upper-middle (levels 10 - 15), lower-middle (levels 5 - 10), bottom (levels 1 - 5), the number of leaflets in each grade, the average leaf area, and the leaf age.

Photosynthesis model (FvCB model)

$A = V_c - 0.5V_o - R_d = \min\{A_c, A_j, A_p\} - R_d$	Net photosynthetic rate	C1
$A_c = V_{cmax}\frac{C_c - \Gamma_*}{C_c + K_c(1 + O/K_o)}$	Rubisco-limited photosynthetic rate	C2
$A_j = \frac{J(C_i - \Gamma_*)}{4(C_i + 2\Gamma_*)}$	RuBP regeneration limited photosynthetic rate	C3
$\theta J^2 - (I_2 + J_{max})J + I_2 J_{max} = 0$	Light dependence of the rate of electron transport	C4
$I_2 = I(1-f)(1-\delta)/2$	PAR effectively absorbed by Photosystem II	C5
$A_p = 3P_u$	TPU limited photosynthetic rate	C6
$K_T = k_{25}\exp\left[E_a(T_p - 25)/\{298R(T_p + 273)\}\right]$	Arrhenius function; temperature dependence of K_c, K_o, R_d, V_{cmax}	C7
$J_{max} = J_{m25}\exp\left[\frac{(T_p - 25)E_a}{R(T_p + 273)298}\right]\frac{\left[1 + \exp\left(\frac{S298 - H}{R298}\right)\right]}{\left[1 + \exp\left(\frac{S(T_p + 273) - H}{R(T_p + 273)}\right)\right]}$	Temperature dependence of J_{max}	C8
$\Gamma^* = 36.9 + 1.88(T_p - 25) + 0.036(T_p - 25)^2$	Temperature dependence of Γ^*	C9
$f(\xi) = d_0(1 - \exp(-d_1\xi))\exp(-d_2\xi)$	Leaf age dependence of J_{max}, V_{cmax} and P_u	C10
$C_i = C_a - A(\frac{1}{g_b} + \frac{1}{g_s})P_a$	Intercellular CO_2 concentration	C11
$C_c = C_i - \frac{A}{g_m}P_a$	Chloroplastic CO_2 concentration	C12
$g_m = \frac{\exp(c - \frac{\Delta H_a}{RT_k})}{1 + \exp(\frac{\Delta S * T_k - \Delta H_d}{RT})}$	Mesophyll conductance to CO_2	C13

Stomatal conductance model (BWB model)

$g_s = b + mA\frac{h_s}{(C_s/P_a)}$	Stomatal conductance	D1
$\Gamma = \frac{R_d(K_c(1 + O/K_o)) + V_{cmax}\Gamma_*}{V_{cmax} - R_d}$	CO_2 compensation point in the presence of R_d	D2
$C_s = C_a - \frac{A}{g_b}P_a$	Estimation of CO_2 partial pressure at the leaf surface	D3
$g_b = 0.147\sqrt{u/d}$ (Gr/Re^2 > 1) $g_b = 0.055 \cdot (\frac{T_p - T_a}{d})^{1/4}$ (Gr/Re^2 < 1) $d = 0.72w$	Boundary layer conductance for water vapor	D4
$a_h h_s^2 + b_h h_s + c_h = 0$ Where $\begin{cases} a_h = (g_1 A)/C_s \\ b_h = g_0 + g_b - (g_1 A/C_s) \\ c_h = (-RHg_b) - g_0 \end{cases}$	Quadratic equation to obtain h_s by combining g_s with diffusion equation	D5

Photosynthetic limitation analysis

$C_{ctr} = \frac{K_c J(K_o + O) - 8K_o\Gamma^* V_{cmax}}{[K_o(4V_{cmax} - J)}$	Value of C_c at the transition point between A_c and A_j.	E1
$\frac{dA}{A} = S_L + M_L + B_L + L_L = A_L$	Total limitation	E2
$\frac{dA}{A} = l_s \times \frac{dg_{sc}}{g_{sc}} + l_m \times \frac{dg_m}{g_m} + l_{bc} \times \frac{dV_{cmax}}{V_{cmax}} + 0 \ (C_c < C_{ctr})$	Total limitation calculation under saturating light conditions	E3
$\frac{dA}{A} = l_s \times \frac{dg_{sc}}{g_{sc}} + l_m \times \frac{dg_m}{g_m} + l_j \times \frac{J_{dt}}{J} + l_j \times \frac{J_{dt}}{J} \ (C_c \geq C_{ctr})$	Total limitation calculation under non-saturating light conditions	E4
$l_s = (\frac{g_{tot}}{g_s} \times \frac{\partial A}{\partial C_c})/(g_{tot} + \frac{\partial A}{\partial C_c})$	Relative limitations of stomatal	E5
$l_m = (\frac{g_{tot}}{g_m} \times \frac{\partial A}{\partial C_c})/(g_{tot} + \frac{\partial A}{\partial C_c})$	Relative limitations of mesophyll conductance	E6
$l_{bc} = g_{tot}/(g_{tot} + \frac{\partial A_c}{\partial C_c})$	Relative limitations of biochemical capacity	E7
$l_j = g_{tot}/(g_{tot} + \frac{\partial A_j}{\partial C_c})$	Relative limitations of electron transport rate	E8
$dA/A \approx (A_{ref} - A)/A_{ref}$		E9
$dg_{sc}/g_{sc} \approx (g_{sc,ref} - g_{sc})/g_{sc,ref}$		E10
$dg_m/g_m \approx (g_{m,ref} - g_m)/g_{m,ref}$		E11
$dV_{cmax}/V_{cmax} \approx (V_{cmax,ref} - V_{cmax})/V_{cmax,ref}$		E12
$J_{dt}/J \approx (J_{s,ref} - J_s)/J_{s,ref}$		E13
$J_{dt}/J \approx (J_s - J)/J_{s,ref}$		E14
		E15
Saturating light condition ($C_c < C_{str}$)		
$A = A_c = V_{cmax} \cdot (C_c - \Gamma^*)/(C_c + K_c \cdot (1 + O/K_o)) - R_d$	Photosynthesis rate in the Rubisco carboxylation-limited stage	E16
$\frac{\partial A}{\partial C_c} = \frac{\partial A_c}{\partial C_c} = \frac{V_{cmax} \cdot (\Gamma^* + K_c(1 + O/K_o))}{(C_c + K_c \cdot (1 + O/K_o))^2}$		E17
$A_{ref} = A_{c,ref} = V_{cmax,ref} \cdot [C_a - \frac{A_{cmax,ref}(1/g_{sc,ref} + 1/g_{m,ref} - \Gamma^*]}{C_a - A_{cmax,ref}(1/g_{sc,ref} + 1/g_{m,ref}) + K_c \cdot (1 + O/K_o)} - R_d$	Reference photosynthesis rate assuming g_{sc}, g_m and V_{cmax} reach their maxima concomitantly.	E18
Non-saturating light condition ($C_c \geq C_{str}$)		
$A = A_j = J \cdot (C_c - \Gamma^*)/(4C_c + 8\Gamma^*) - R_d$	Photosynthesis limited by electron transport rate	E19
$\frac{\partial A}{\partial C_c} = \frac{\partial A_j}{\partial C_c} = \frac{V_{cmax} \cdot (\Gamma^* + K_c(1 + O/K_o))}{(C_c + K_c \cdot (1 + O/K_o))^2}$		E20
$A_{ref} = A_{j,ref} = J_{s,ref} \cdot [C_a - \frac{A_{j,ref}(1/g_{sc,ref} + 1/g_{m,ref} - \Gamma^*]}{C_a - A_{cmax,ref}(1/g_{sc,ref} + 1/g_{m,ref}) + K_c \cdot (1 + O/K_o)} - R_d$	Photosynthesis rate with maximum J_{max}.	E21

Verification of the Simulation Model for the Photosynthetic Rate of Tomato Leaves in Solar Greenhouses.

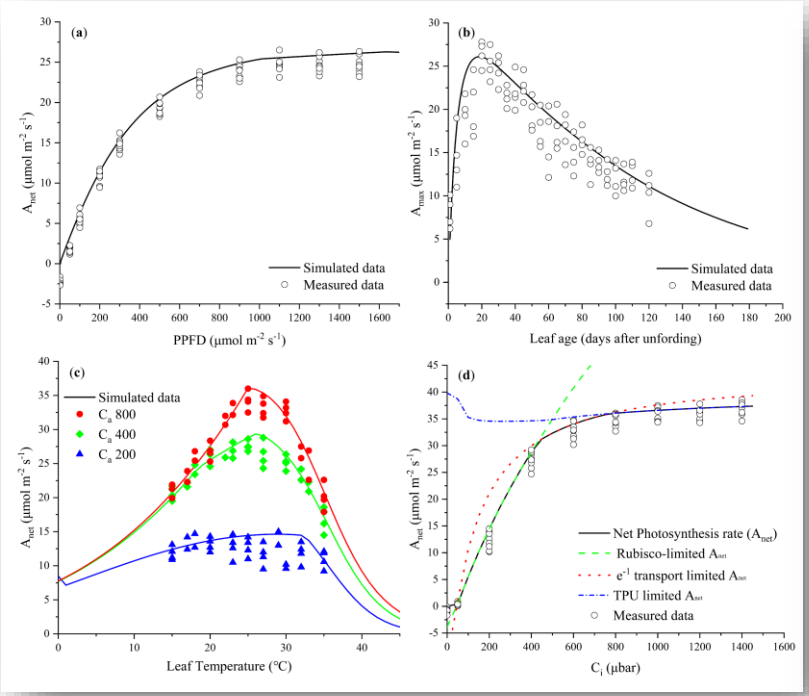

Calibration of the extended K&L module to the PAR response curve (a) and the Amax to leaf age response curve (b); (c), verification of leaf temperature to A under three different Ca concentration levels (200, 400, 800 μbar); (d), A/Ci response curve.

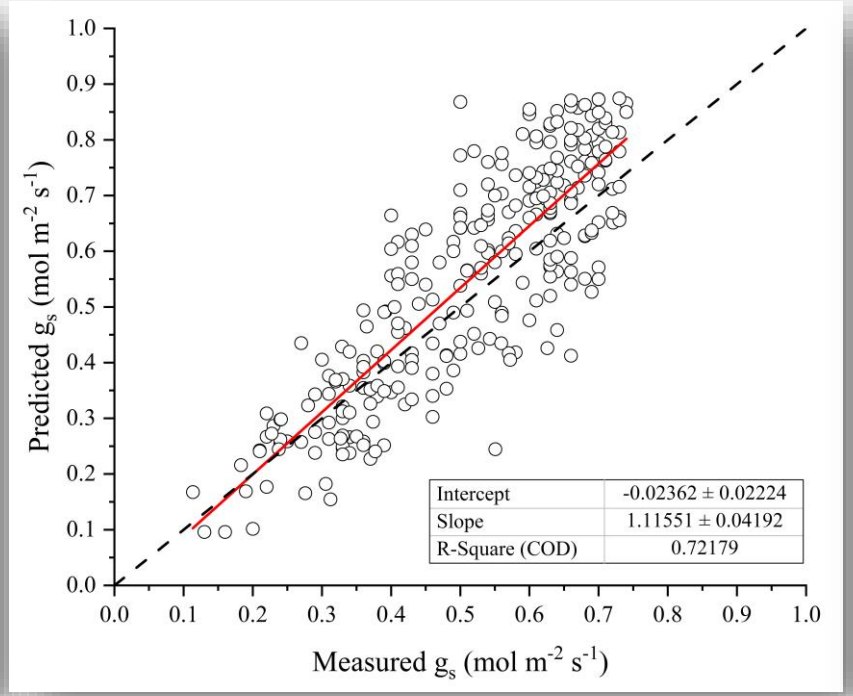

Linear regression of the predicted g_s values against the measured g_s values as a result of the calibration of the BWB model. The dashed line represents a one-to-one relationship.

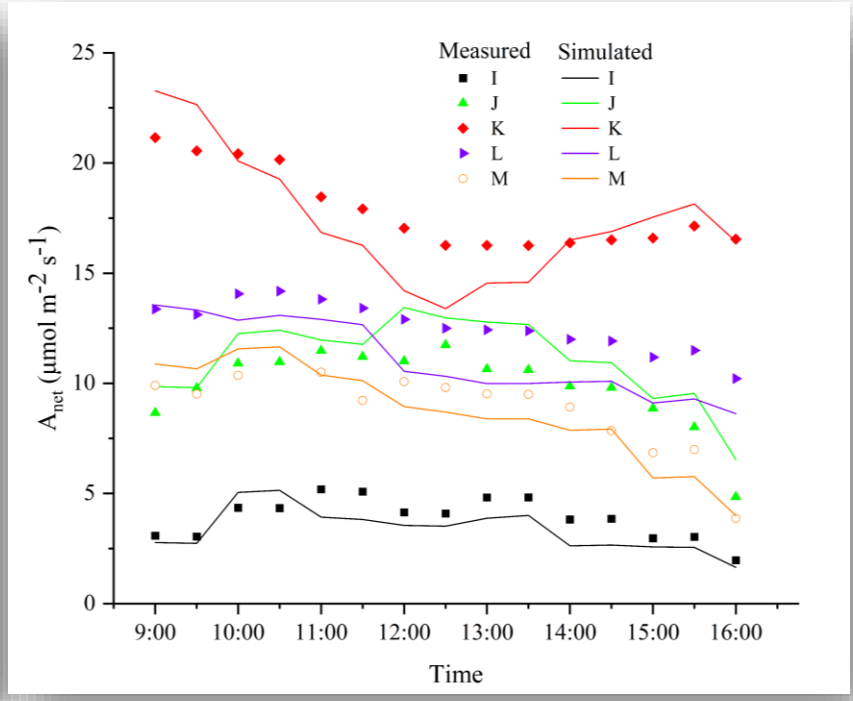

Verification of the spatial distribution of photosynthesis of leaflets at the five points (I - M) shown in Figure 3 at 12:00 noon.

Contents

Classification of the Structures of Energy-saving Solar Greenhouses.

Divide the solar greenhouse into two parts by the cross-section:

- The front half (A - B - C).
- The rear half (B - D - E - C).

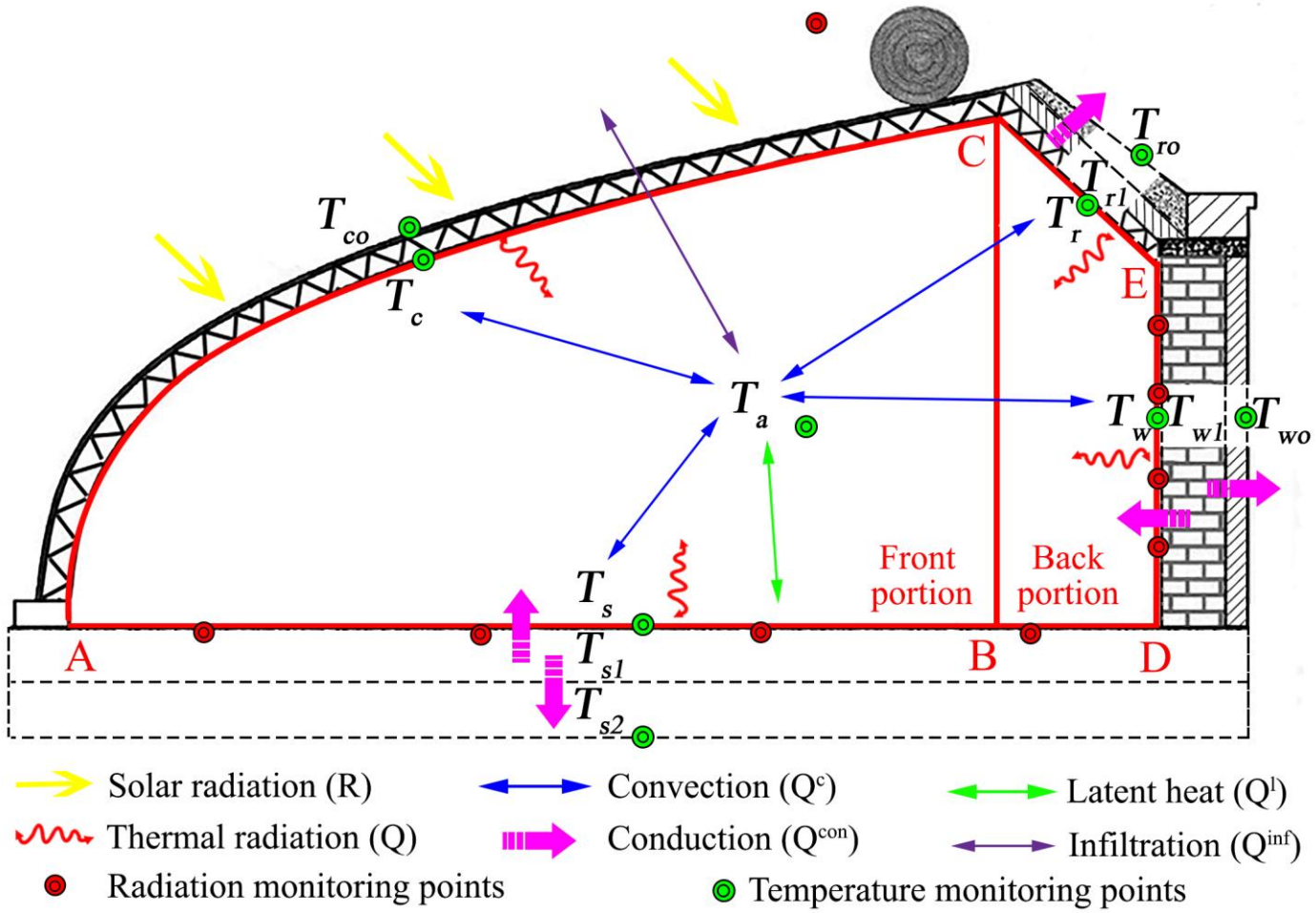

Cross-sectional views of the front part (A - B - C) and the rear part (B - D - E - C) of the experimental greenhouse, corresponding to the monitoring points of energy flux, radiation, and temperature at different parts of the solar greenhouse. AB represents the width of the front part; BC represents the ridge height; DE represents the height of the north wall; and BD represents the horizontal projection of the rear roof.

Simulation of the Intermediate Difference in the Front Structure of Energy-saving Solar Greenhouses: (Front Morphology Model)

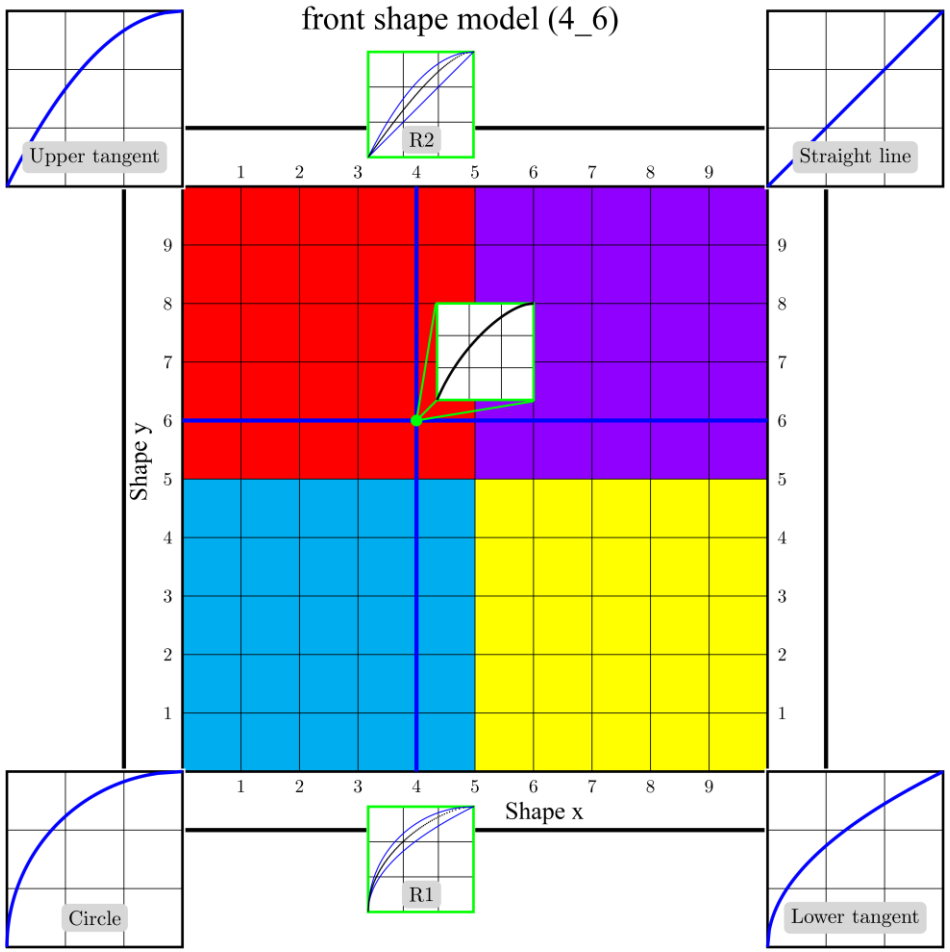

Simulation diagrams of the intermediate difference situations of the front half shapes of four extreme greenhouses. The four corners of the graph correspond to the four extreme shape situations respectively.

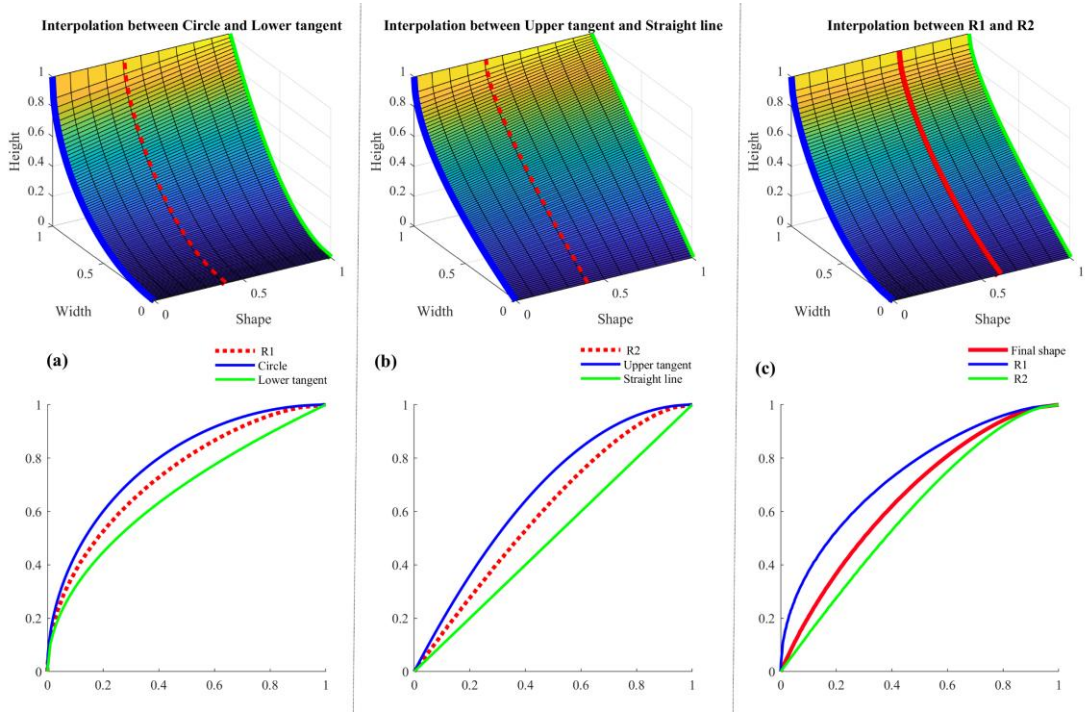

The bilinear fitting process of the front roof shape model front shape 4_6 under the specific conditions of 40% on the X-axis and 60% on the Y-axis. The upper part of the figure shows the 3D spatial changes in each interpolation step. The two-dimensional graphics below are the curves involved in the interpolation steps of the example front shape 4_6.

Mathematical formulas for the four extreme values of the front roof shapes.

Shapes	Circle	Lower tangent parabolic	Upper tangent parabolic	Straight-line
Height	6	2	10	6
Width	6	10	2	6
Equation	$x^2 + y^2 = 1$	$y^2 = x$	$y = (x-1)^2+1$	$y = x$

Simulation of the Intermediate Difference of Parameters in the Front and Rear Parts of Energy-saving Solar Greenhouses: (Front and Rear Structure Parameter Models)

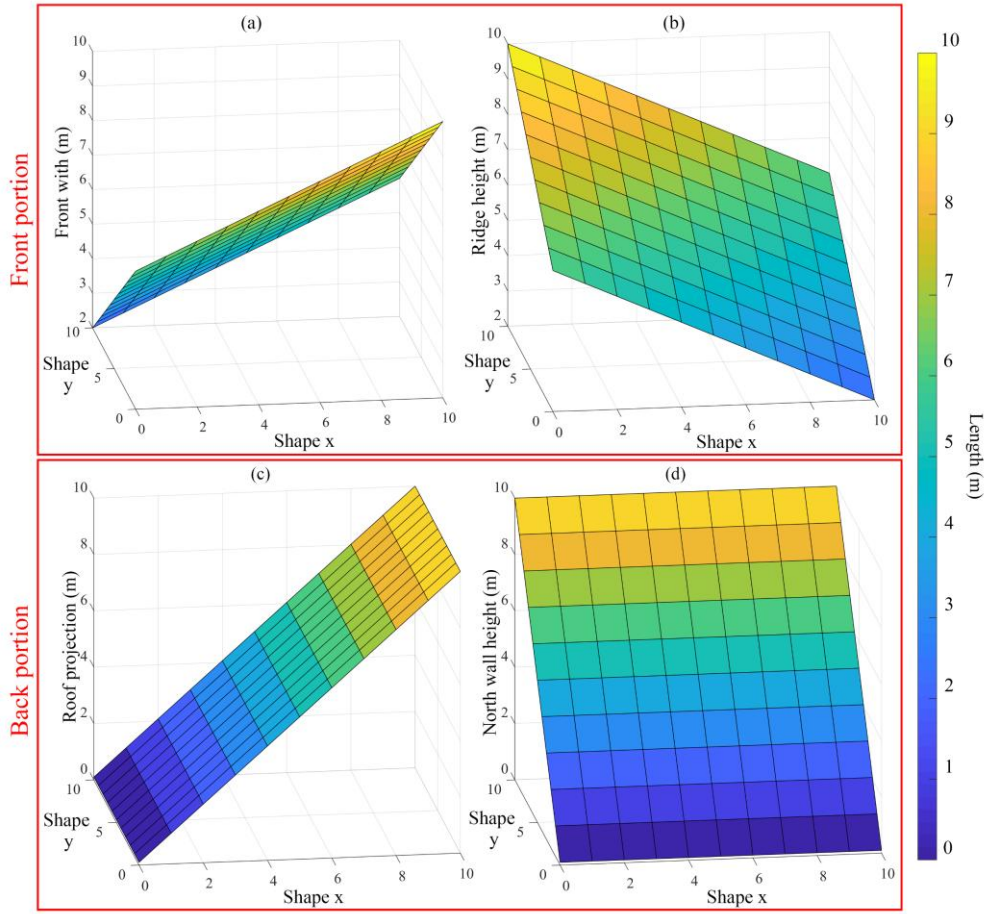

The size model interpolations of front width (AB) (a) and ridge height (BC) (b) for each shape configuration of the four greenhouse front portion extrema. Interpolations of north roof projection (BD) (c) and north wall height (DE) (d) for each shape configuration of the greenhouse back portion corresponding with each specific front portion (X_Y).

The front structure of the solar greenhouse is a combination of the front morphological structure model and the front parameter model.

front portion (X_Y) = (front width (x_y), ridge height (x_y)) × front shape model (x_y)

The rear structure of the solar greenhouse is the rear parameter model.

back portion (X_Y) = north roof projection (x_y), north wall (x_y)

3.1 Simulation of the Structure of Solar Greenhouses

Simulation of the Optimal Greenhouse Structure:

A total of 121 (11 × 11) different front greenhouse structures.

A total of 121 (11 × 11) different rear greenhouse structures.

Sum up to 14,641 (121 × 121) greenhouse structures were simulated in this study.

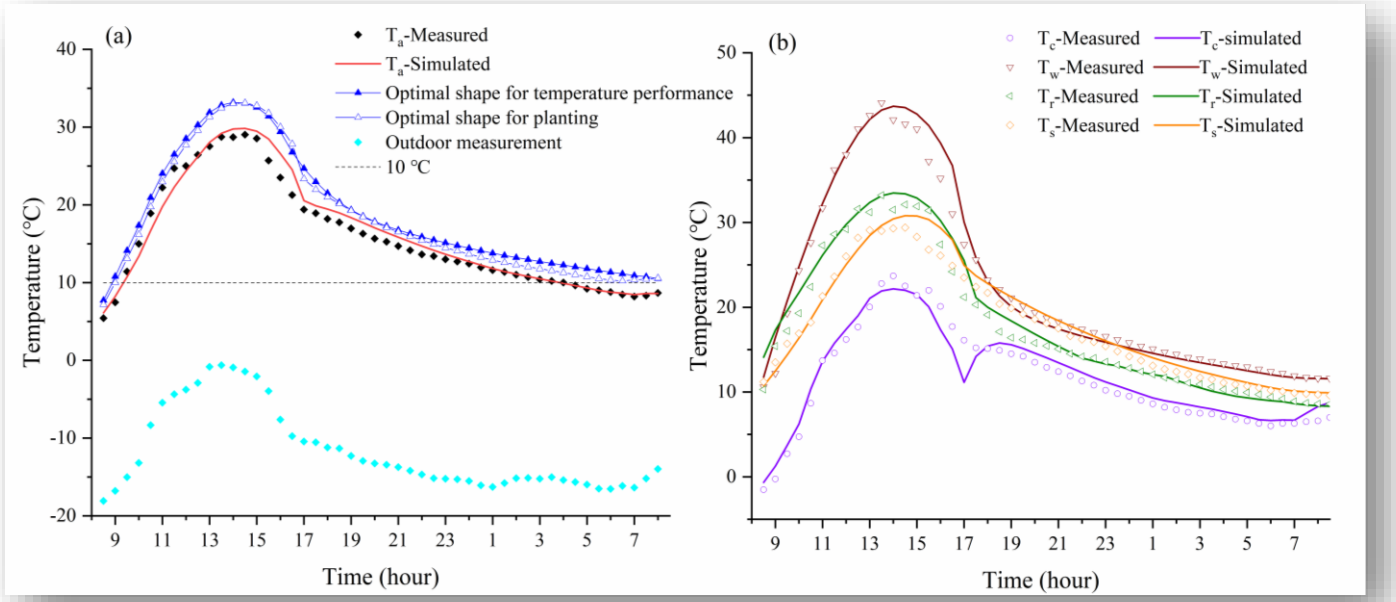

Temperature verification (measured values and simulated values) of the heat balance module of the greenhouse 3D simulation model, including the verification of the indoor temperature of the experimental greenhouse (Figure a) and the verification of the internal surface temperatures of the front roof (Tc), the north wall (Tw), the rear slope (Tr), and the soil (Ts) (Figure b). And the temperature performance of the two best energy-saving solar greenhouses finally obtained from the simulation (the solid triangle represents the greenhouse with the best thermal performance, and the hollow triangle represents the greenhouse with the best thermal performance for optimizing the planting space).

Root Mean Square Error (RMSE) between the measured values and the simulated values of temperature prediction by the heat balance expansion module and the correlation coefficient (r) between the simulated values and the measured values.

	T_a	T_c	T_w	T_r	T_s
RMSE	1.1802	1.3270	1.5604	1.4308	1.2242
r	0.9680	0.9203	0.9638	0.9588	0.9592

Simulation of the Front Structure of Energy-saving Solar Greenhouses:

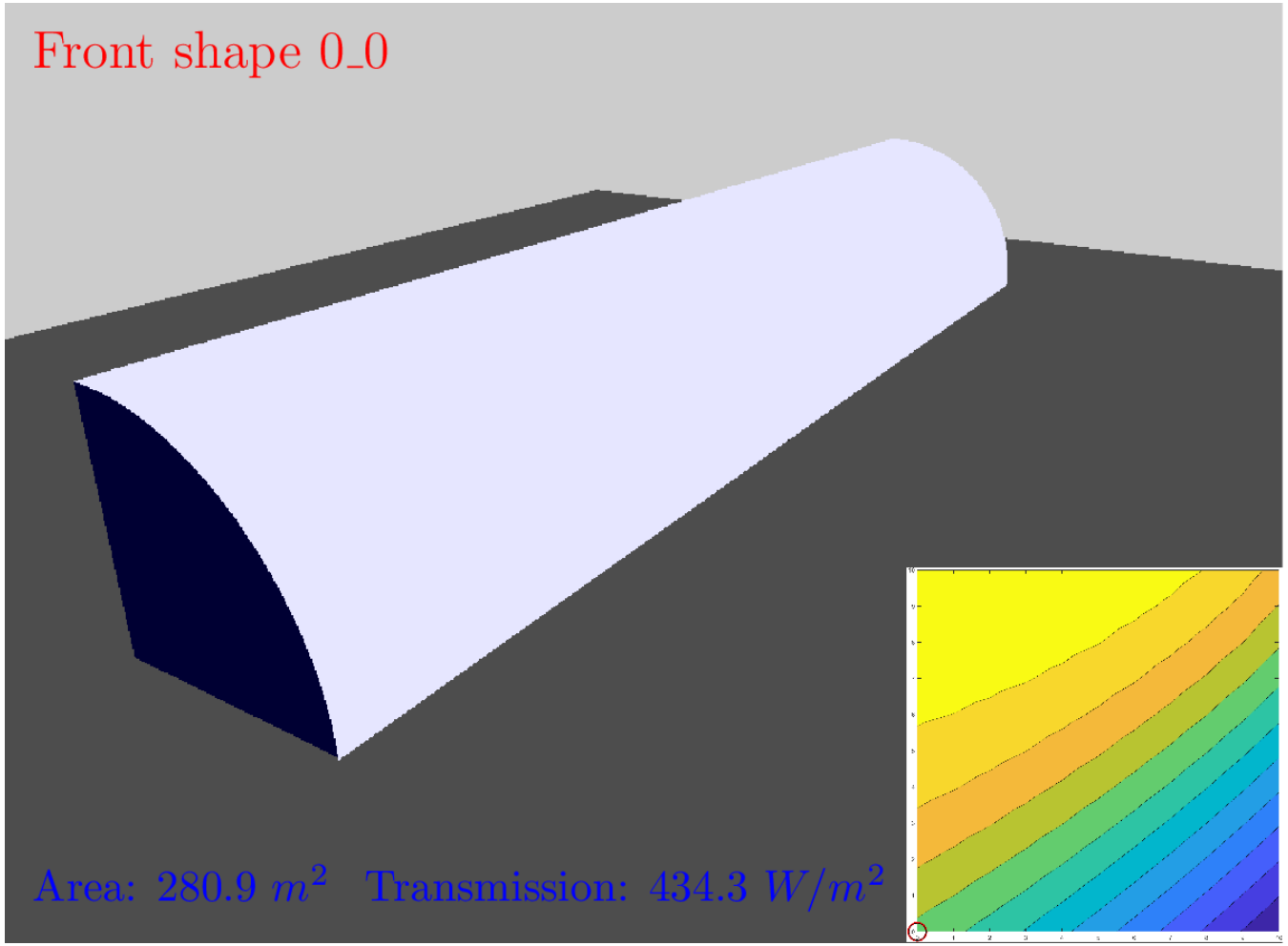

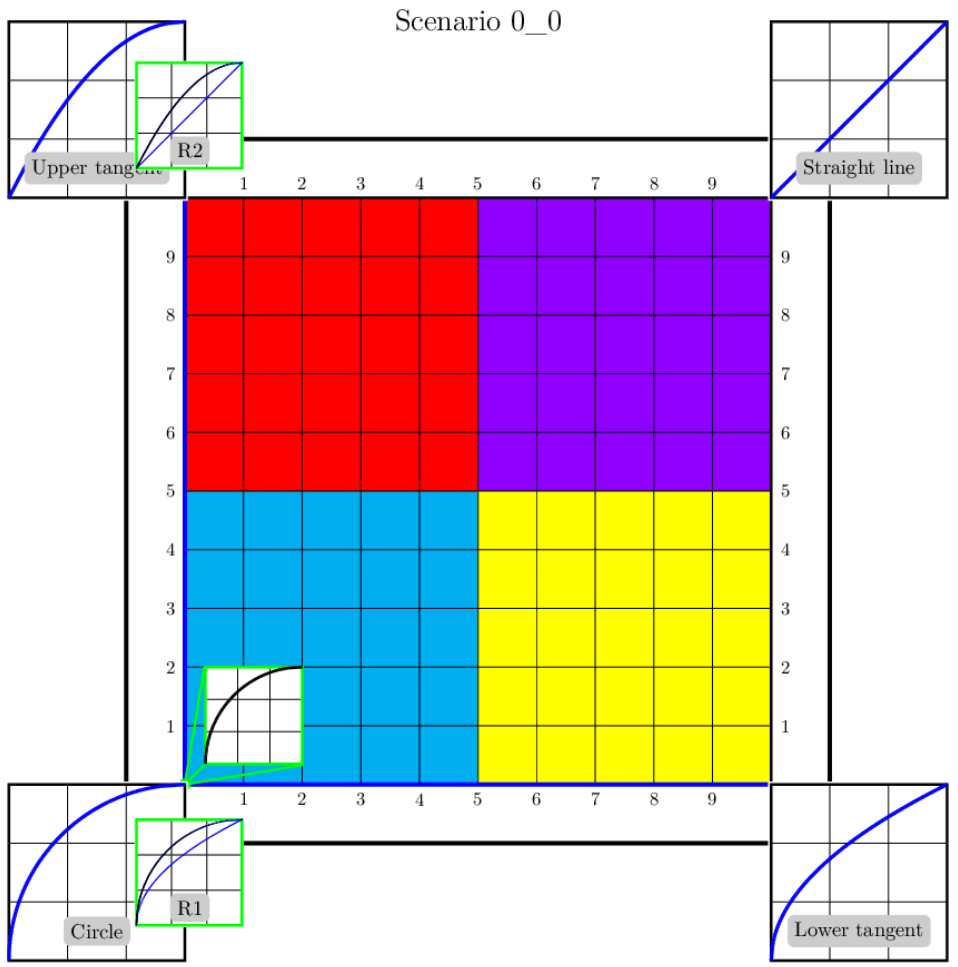

Demonstration of the Scene Simulation of the Front Structure of the Greenhouse.

Simulation of the Rear Structure of Energy-saving Solar Greenhouses:

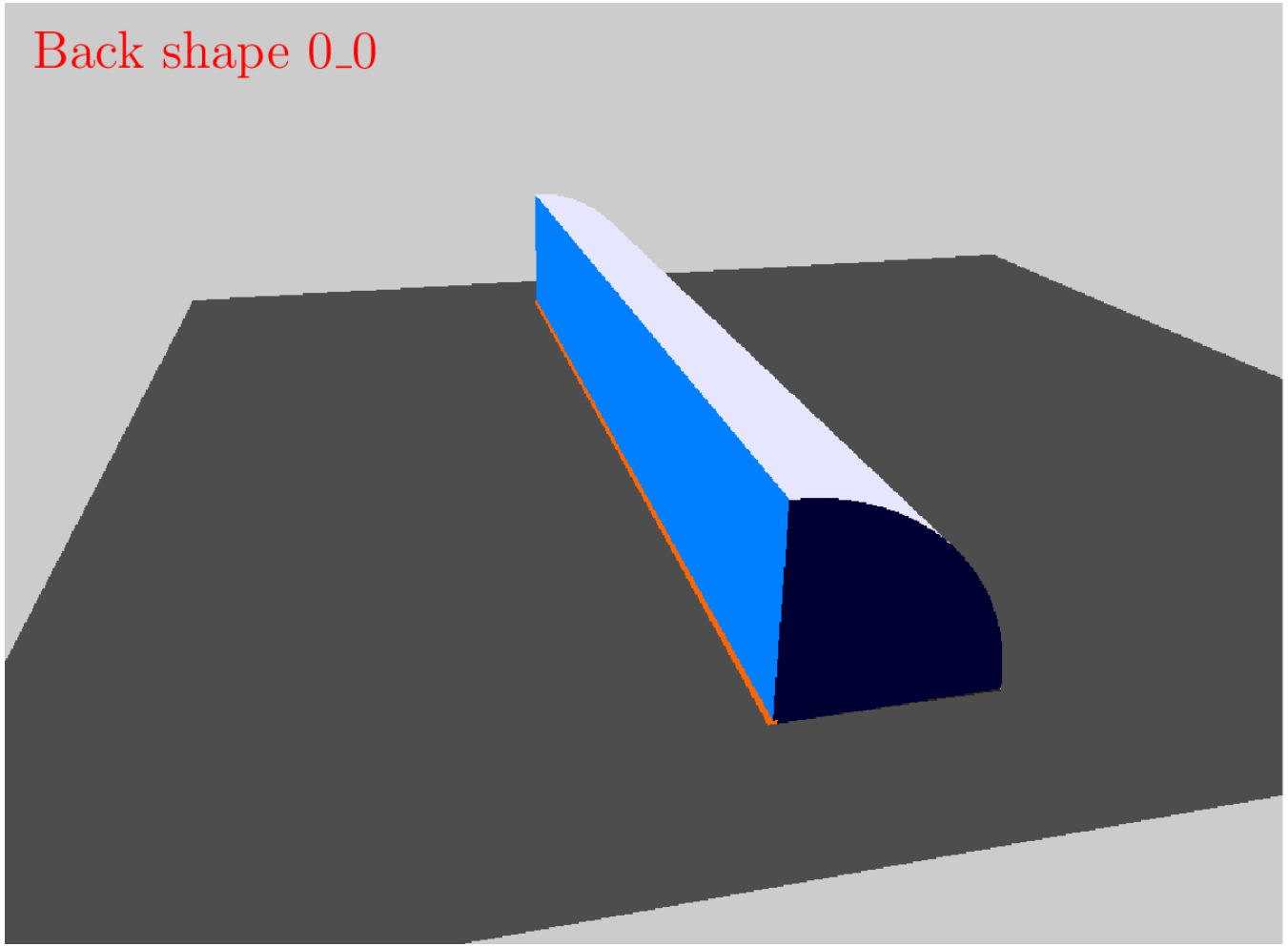

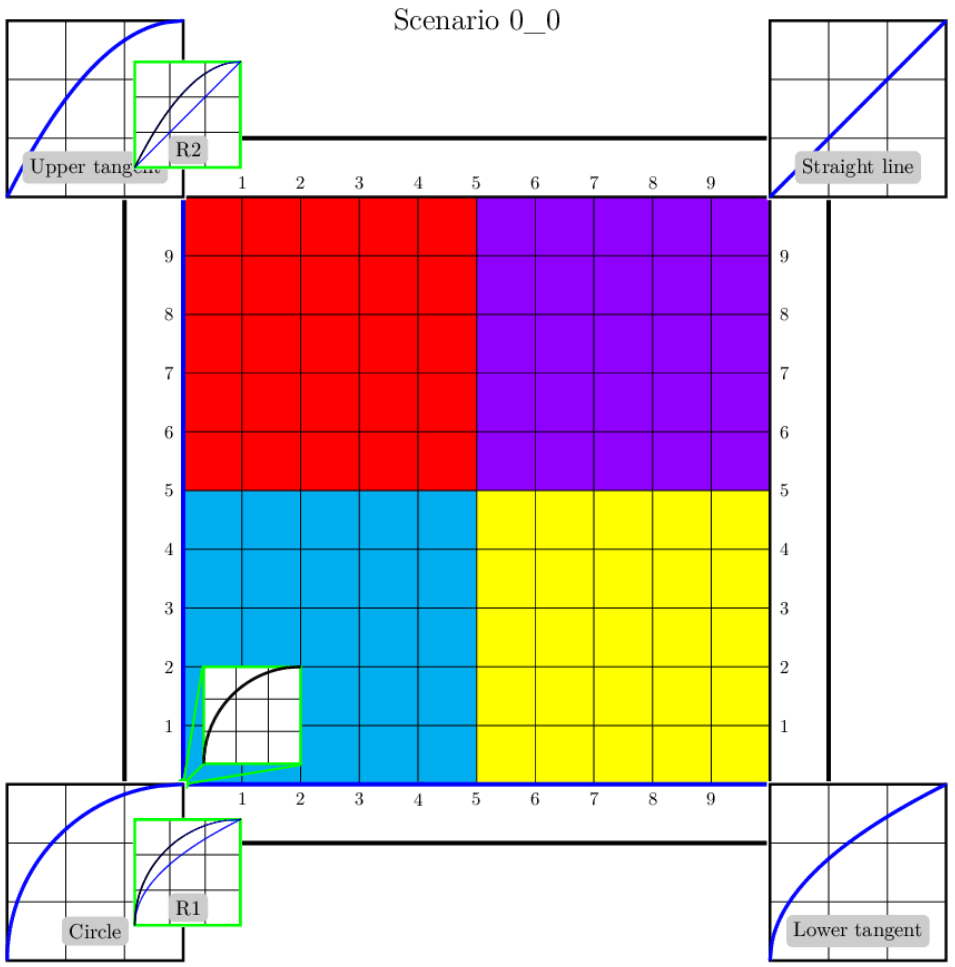

Demonstration of the Scene Simulation of the Rear Structure of the Greenhouse.

Analysis of Light Radiation in the Front Structure of Energy-saving Solar Greenhouses:

Total amount of solar radiation transmitted through the front roof

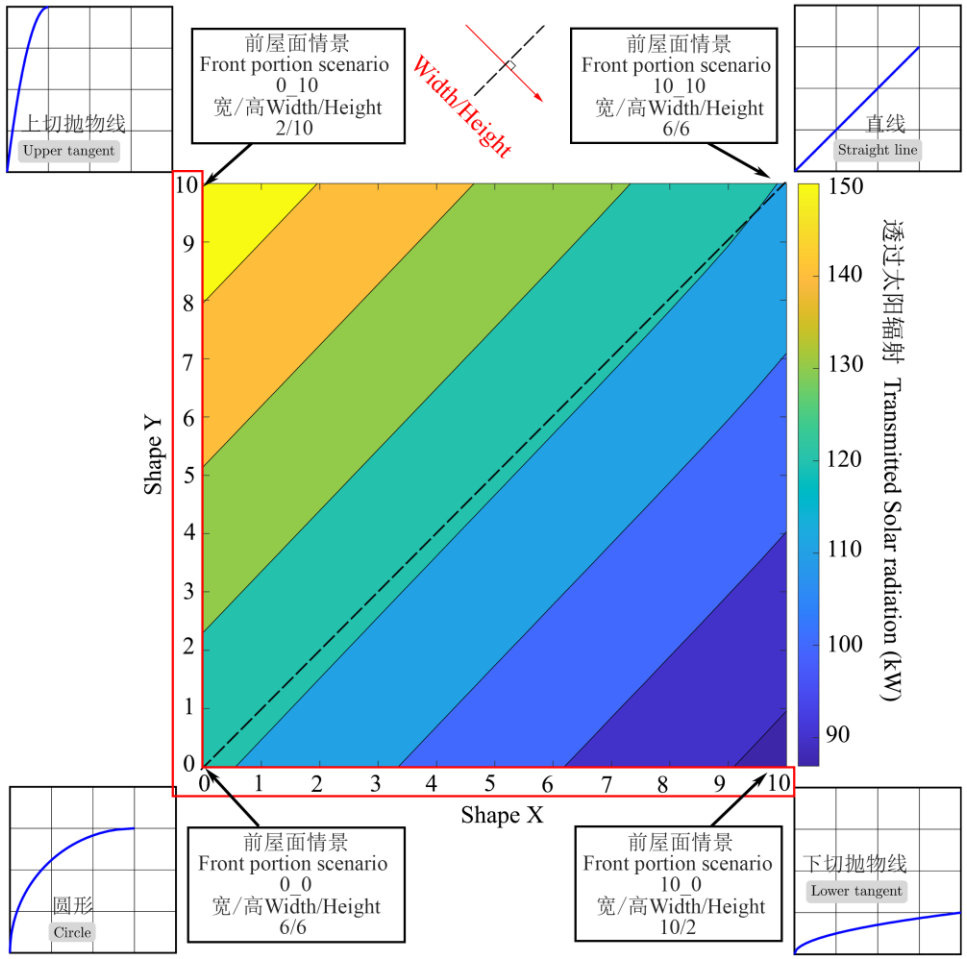

The total daily solar radiation (A) and the amount of solar radiation per unit area (B) transmitted through the front roof surface (AC) under each interpolation simulation scenario of the front structure of the greenhouse. The dashed diagonal lines represent all scenarios of the front structure of the greenhouse where the width of the front part of the greenhouse and the ridge height have the same value (6 m), and are perpendicular to the direction of the increase in the front width/ridge height (AC/BC) (indicated by the red arrow).

Analysis of Light Radiation Entering the Front Structure of Solar Greenhouses:

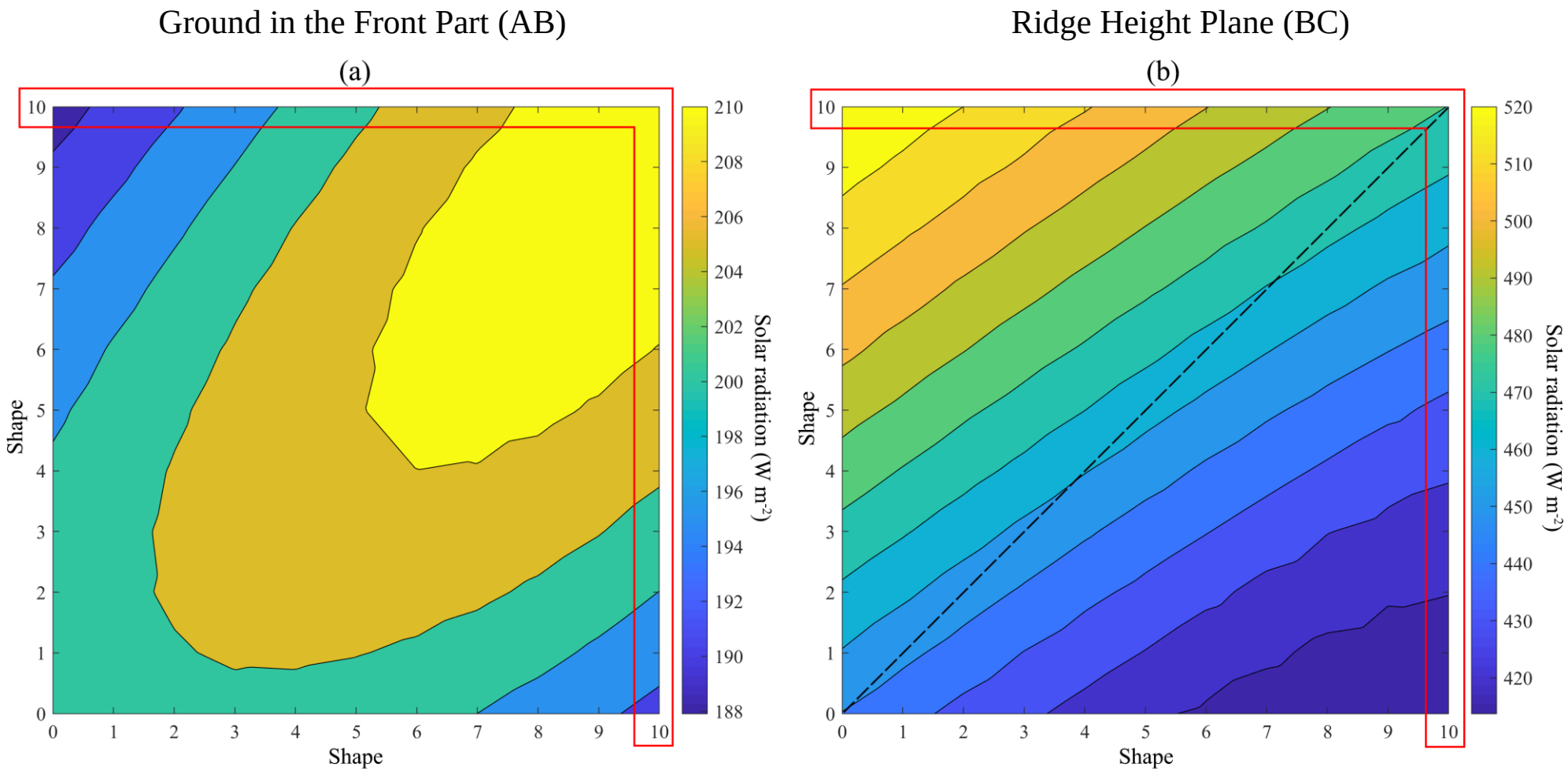

Simulation results of the average daily solar radiation intensity per unit area reaching the ground in the front part of the greenhouse (AB, Figure a) and the ridge height plane (BC, Figure b) under each scenario of the front structure of the greenhouse. The direction of the dashed lines indicates the front structure of the greenhouse where the front width and the ridge height have the same values. The red boxes at the top and on the right side of each sub-figure represent the front structure of the greenhouse with better light interception performance.

Analysis of Light Radiation in the Front Structure of Energy - saving Solar Greenhouses:

Select the circular front roof (front portion(0_0)) and the straight front roof (front portion(10_10)) to conduct a detailed comparison of the solar radiation distribution on the AB surface and the BC surface.

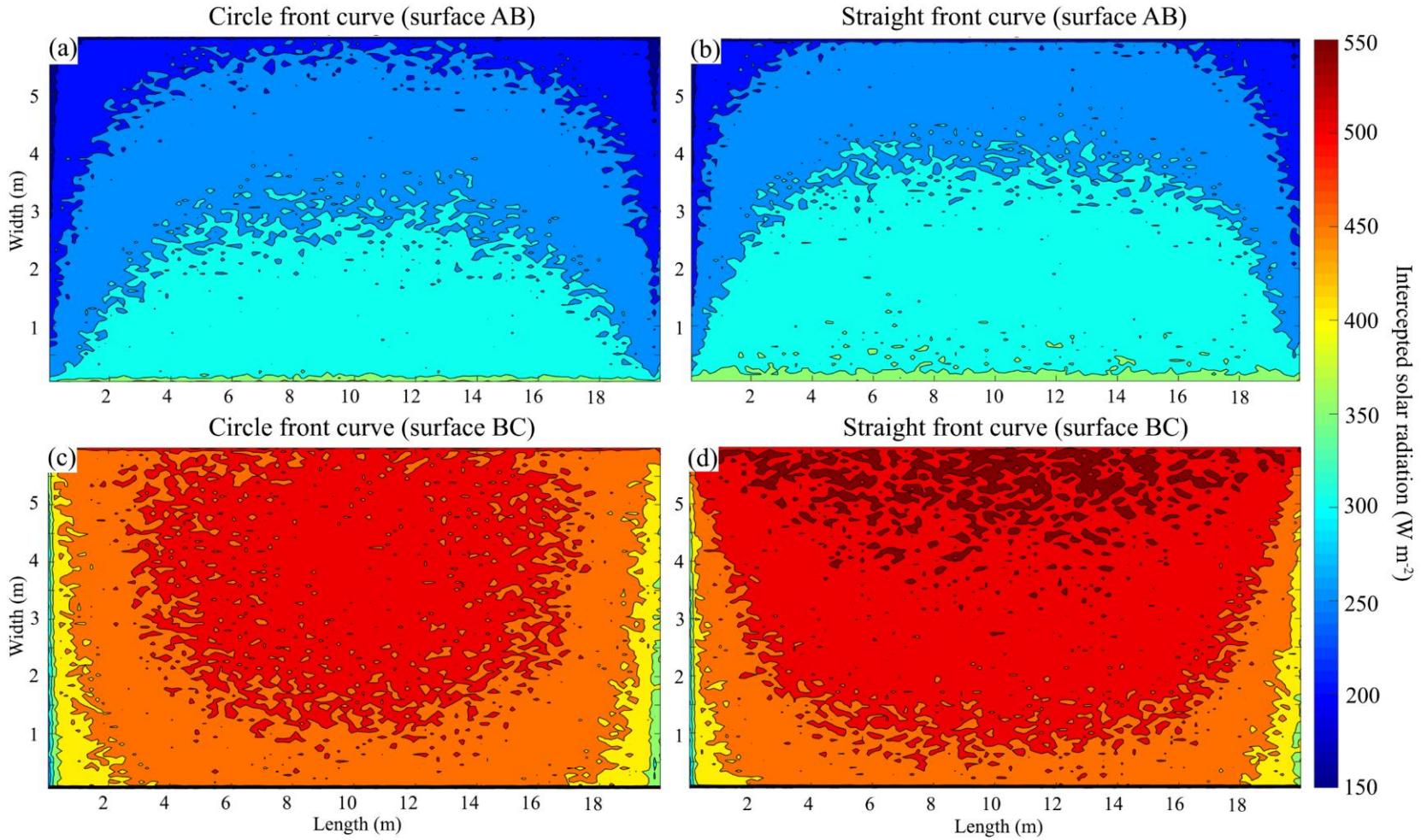

Comparison of the simulated values of the solar radiation distribution reaching the front structure of the circular greenhouse (front portion(0_0), Figures a, c) and the front structure of the straight-line greenhouse (front portion(10_10), Figures b, d) at 12 noon on the winter solstice. Among them, Figures a and b show the distribution of light radiation interception on the ground in the front part of the greenhouse, and Figures c and d show the distribution of light radiation on the ridge height plane of the greenhouse.

Automatic Optimization and Screening of the Structure of Energy - saving Solar Greenhouses:

Greenhouse Front Scenarios Meeting the Screening Conditions:

① The minimum indoor air temperature ≥ 10 °C.

② The total span of the greenhouse ≥ 8 m

③ Ridge height (BC) ≥ the height of the north wall (DE).

④ Select the minimum height of the north wall.

⑤ Select the maximum horizontal projection of the rear slope.

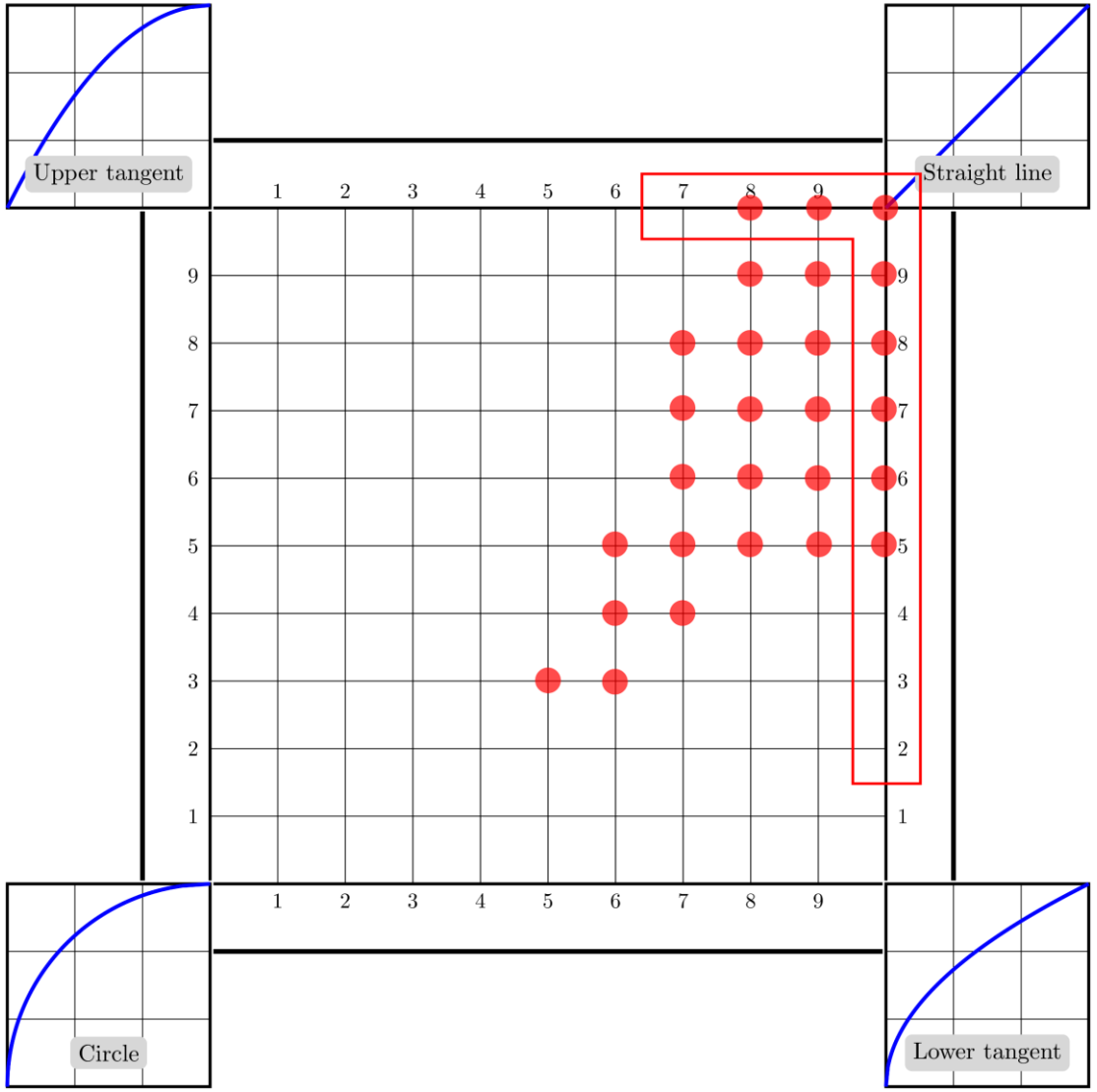

The front structure scenarios of the greenhouse that meet the minimum requirements for the optimal greenhouse structure, which are automatically screened out through programming, are indicated by red dots. The red rectangles represent the 12 selected front scenarios (used to illustrate the screening process of the rear part of the greenhouse, corresponding to Figure 25) as examples.

3.2 Analysis of the Structure of Solar Greenhouses

The Screening Process of the Rear Structure of Energy-saving Solar Greenhouses:

Same Screening Conditions:

① The minimum indoor air temperature ≥ 10 °C.

② The total span of the greenhouse ≥ 8 m

③ Ridge height (BC) ≥ the height of the north wall (DE).

④ Select the minimum height of the north wall.

⑤ Select the maximum horizontal projection of the rear slope.

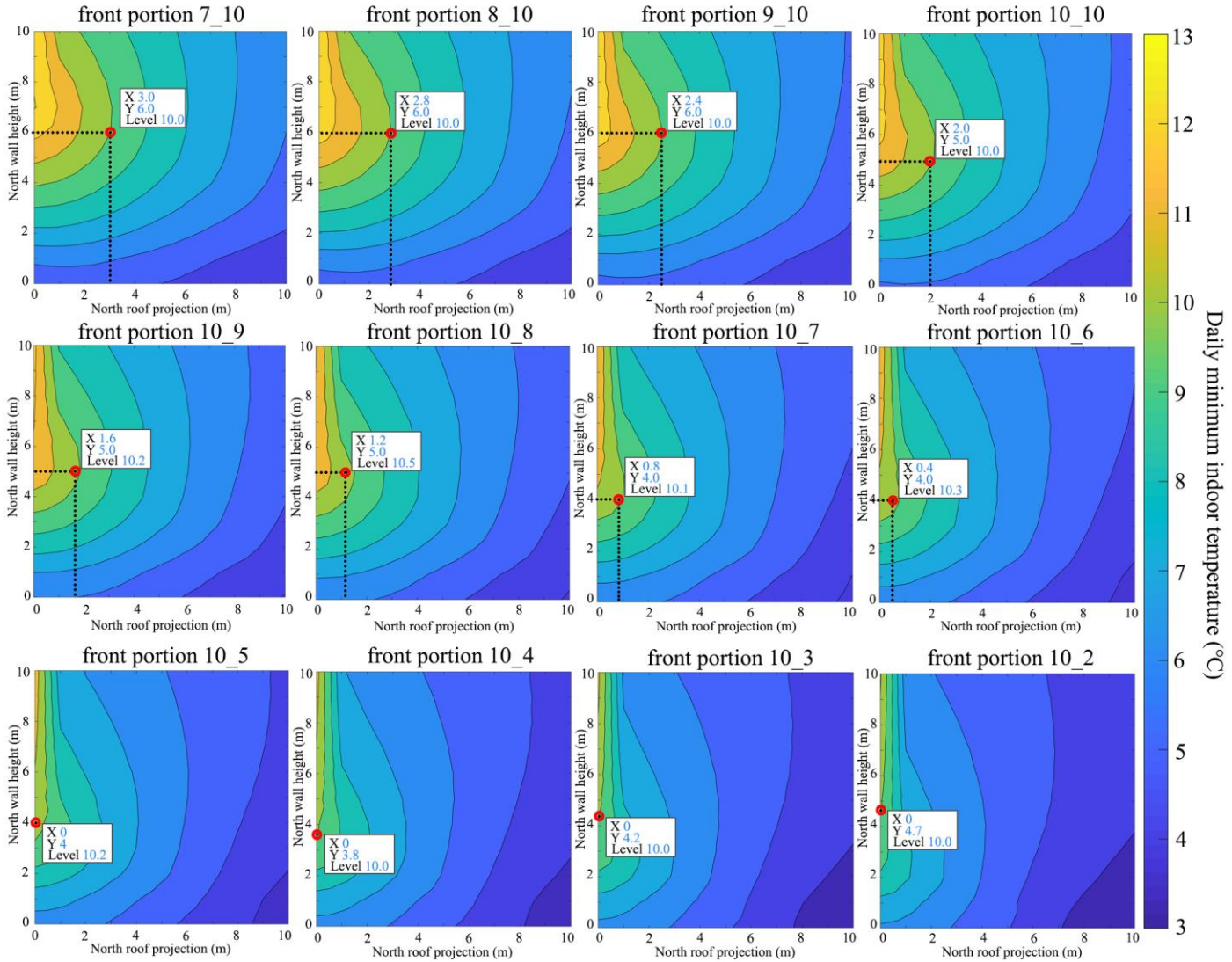

The intermediate difference scenarios of different greenhouse rears corresponding to each selected greenhouse front scenario (corresponding to the front structure scenarios of the greenhouse boxed by the red rectangles in Figure 3 - 10) are represented by the simulated values of the daily minimum indoor temperature of the greenhouse. Only the parameter value scenarios with the total width of the greenhouse (AD) ≥ 8 m, the minimum indoor temperature \(T_{a}^{\min}\) ≥ 10 °C, and the highest minimum temperature at night are selected. The red circles represent the optimal greenhouse rear structure parameters (with the longest horizontal projection of the rear slope and the lowest height of the north wall) corresponding to each greenhouse front scenario (X_Y).

Optimization Analysis of the Structure of Energy - saving Solar Greenhouses:

Among the 14,641 greenhouse structure scenarios, the improved greenhouse structures that meet the conditions through conditional programming will be listed in Table 5.

Table of greenhouse construction parameters that meet the minimum parameter requirements of energy-saving solar greenhouses in Shenyang area corresponding to the front structure of the greenhouse in Figure 31. The four best shapes for nocturnal thermal performance and better planting conditions are highlighted in pink. The values highlighted in red indicate the unqualified marginal shapes.

Front portion scenario	Front width (m)	Ridge height (m)	Roof projection (m)	Wall height (m)	Width (m)
7_10	4.8	7.2	3	6	7.8
8_10	5.2	6.8	2.8	6	8.0
7_8, 8_9, 9_10	5.6	6.4	2.4	6	8.0
7_7, 8_8, 9_9, 10_10	6	6	2.0	5	8.0
6_5, 7_6, 8_7, 9_8, 10_9	6.4	5.6	1.6	5	8.0
5_3, 6_4, 7_5, 8_6, 9_7, 10_8	6.8	5.2	1.2	5	8.0
6_3, 7_4, 8_5, 9_6, 10_7	7.2	4.8	0.8	4	8.0
9_5, 10_6	7.6	4.4	0.4	4	8.0
10_5	8	4	0	4	8.0
10_4	8.4	3.6	0	3.8	8.4
10_3	8.8	3.2	0	4.2	8.8
10_2	9.2	2.8	0	4.7	9.2

3.2 Analysis of the Structure of Solar Greenhouses

Optimized and Improved Structures of Energy-saving Solar Greenhouses:

$$y = -0.8344x^2 + 1.7071x + 0.1074 \qquad R^2=0.996$$

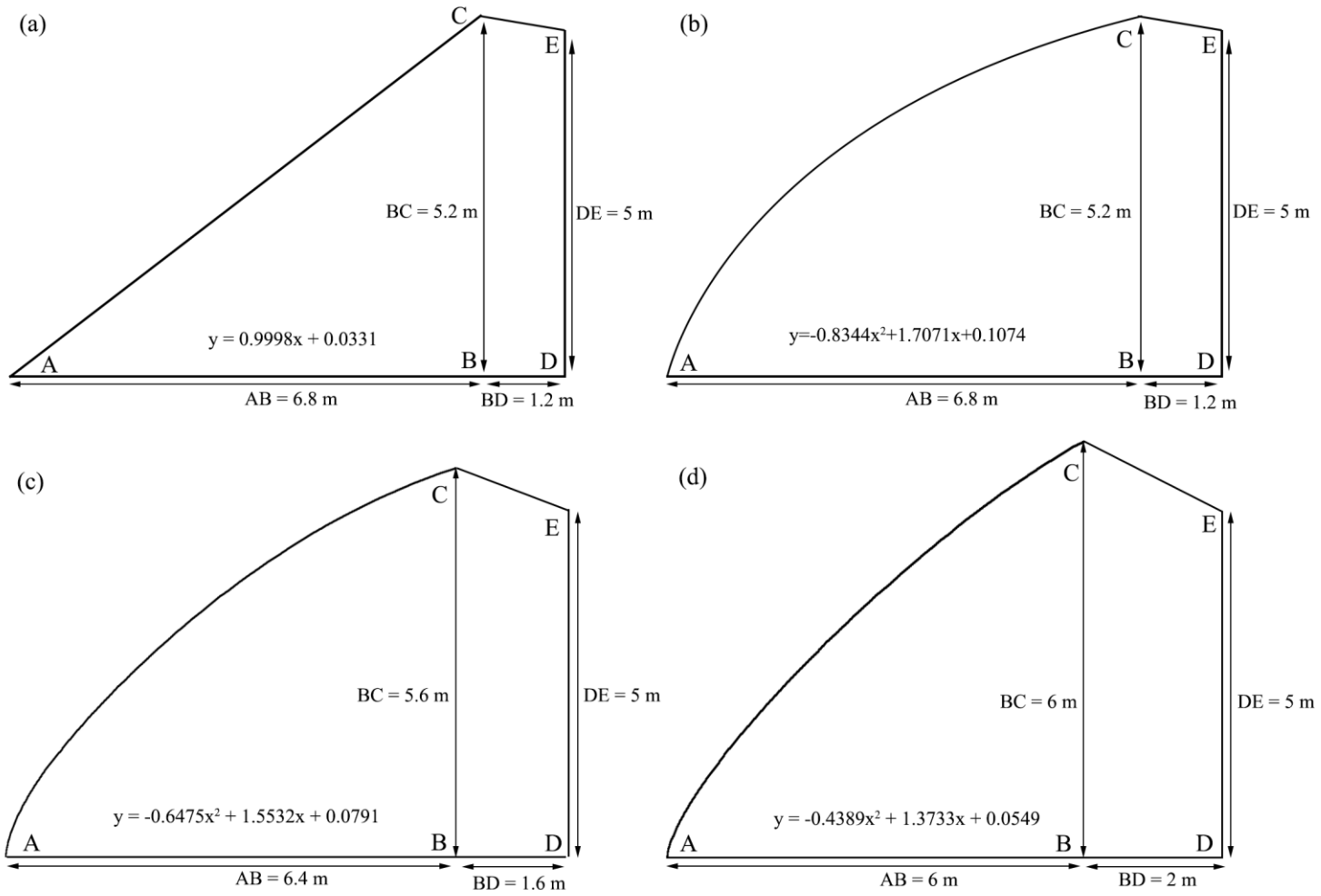

Simulated sectional views of the improved solar greenhouse structure with better nocturnal temperature performance in Shenyang area (a), and the three improved greenhouses with larger planting spaces (b, c, d), along with the polynomial equations of their corresponding front greenhouse morphological models.

3.2 Analysis of the Structure of Solar Greenhouses

Analysis of the Simulated Values of Structural Parameters of Energy-saving Solar Greenhouses:

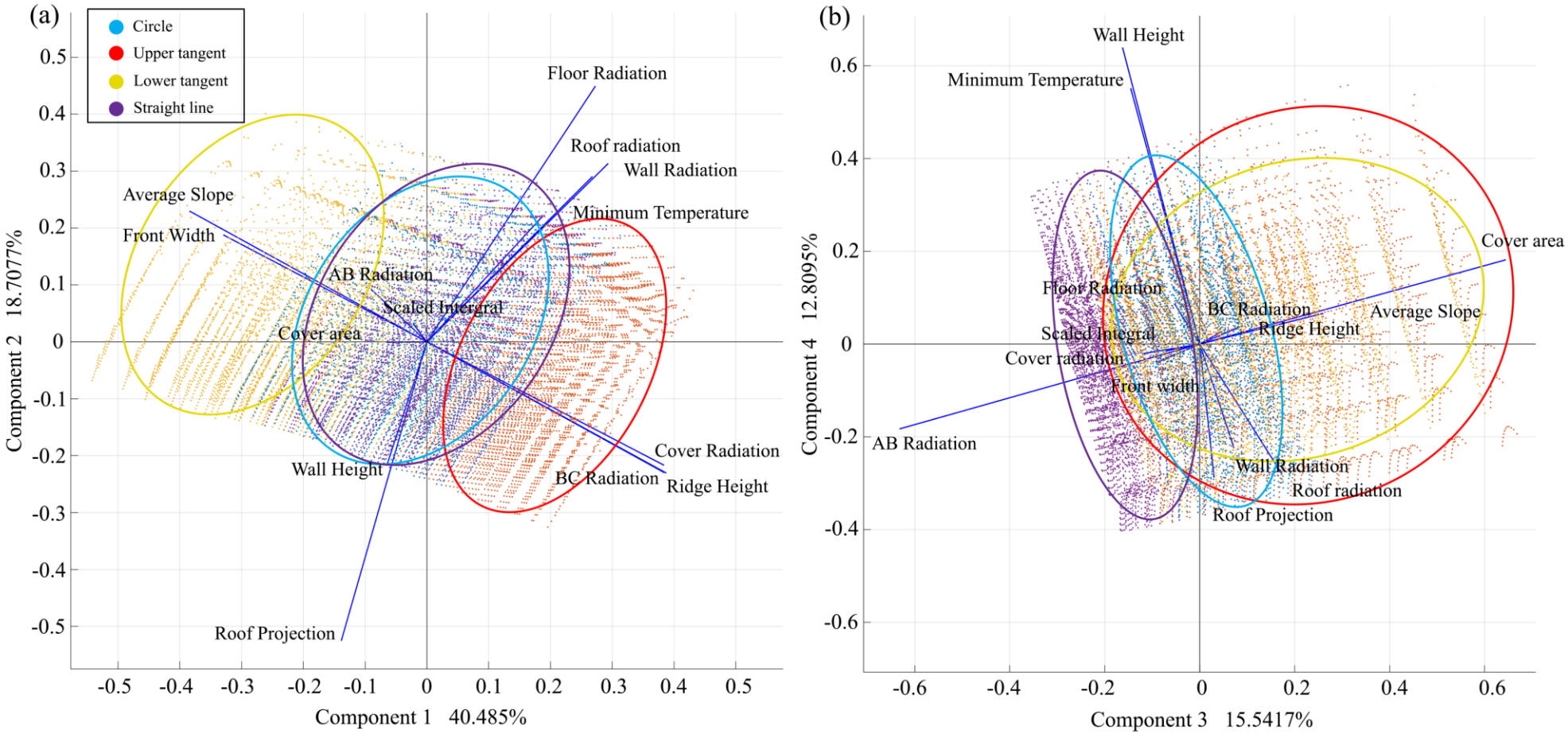

Figure 29. Results of principal component analysis on the light and thermal performance of energy-saving solar greenhouses with respect to the building structural parameter indicators. Figure (a) shows the first and second principal components, and Figure (b) shows the third and fourth (b) principal components.

Contents

4.1 Simulation Analysis of the Light Environment

Simulation Analysis of Light Distribution in Energy-saving Solar Greenhouses:

Light distribution on the surface of the rear wall (upper part in Figure) and the soil surface (lower part in Figure) of the solar greenhouse.

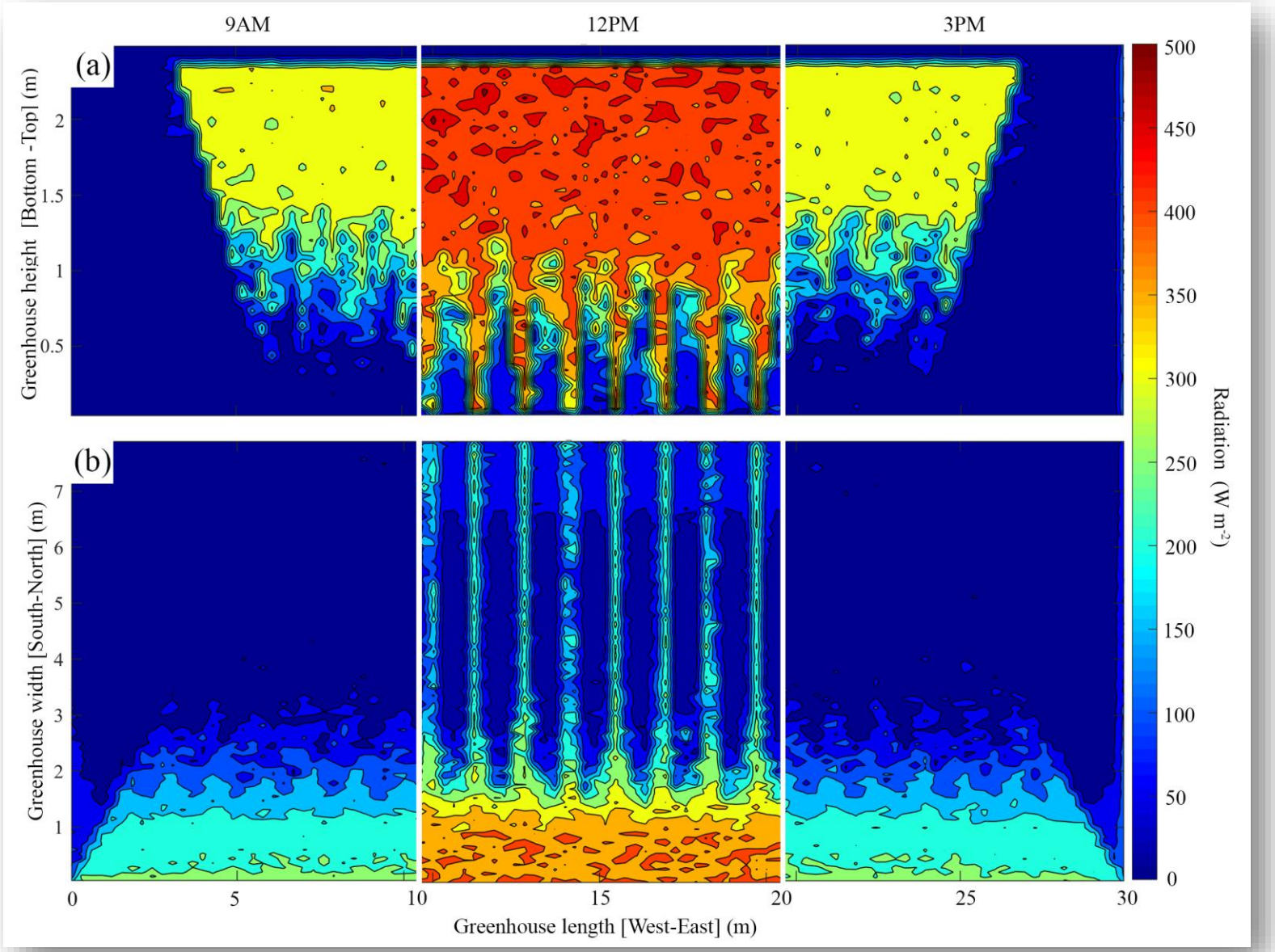

Schematic diagrams of the distribution patterns of solar radiation energy on the north wall (a) and the ground (b) in the tomato greenhouse at 9:00 am, 12:00 noon, and 3:00 pm as simulated.

4.2 Simulation Analysis of the Thermal Environment

Simulation Analysis of Light Distribution in Energy-saving Solar Greenhouses:

Temperature distribution on the surface of the rear wall (upper part in Figure) and the soil surface (lower part in Figure) of the solar greenhouse.

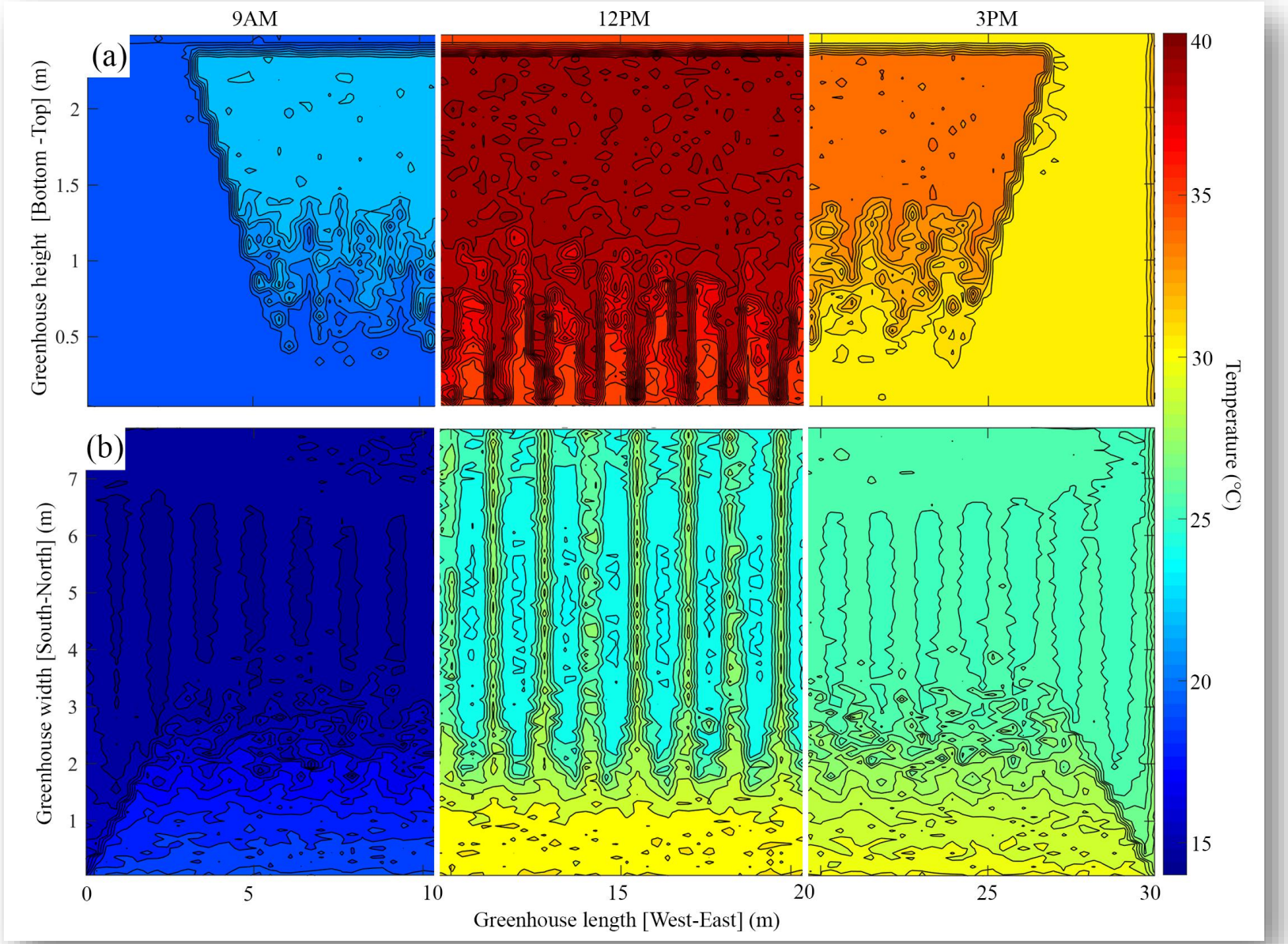

Figure 31. Schematic diagrams of the temperature distribution patterns of the north wall (a) and the ground (b) in the tomato greenhouse at 9:00 am, 12:00 pm (noon), and 3:00 pm as simulated.

4.3 Analysis of the Microclimate on Tomato Leaf Surfaces

Simulation of the Light and Temperature Distribution in Tomato Populations

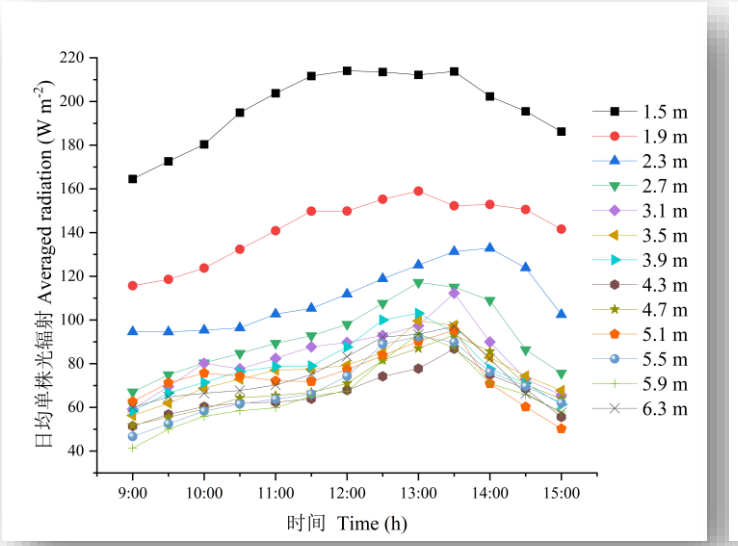

Daily intercepted light radiation of a single tomato crop at the cross-section in the middle of the greenhouse, which is (1.5 - 6.3 m) away from the southern bottom corner of the greenhouse.

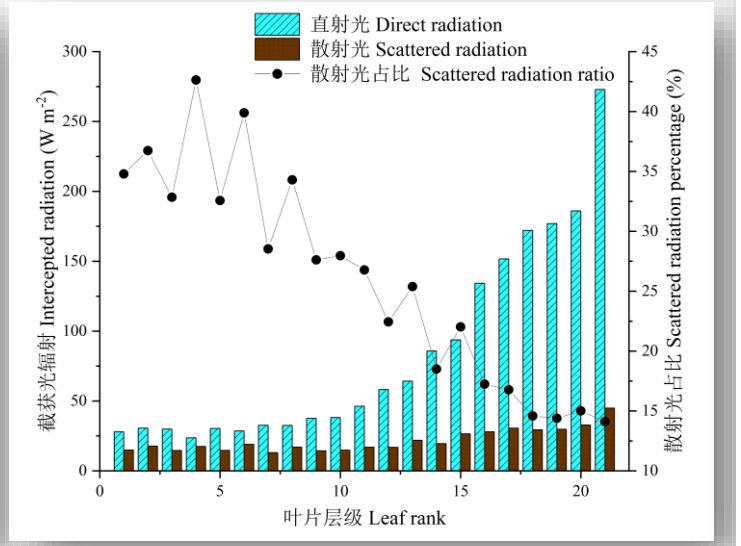

The daily average direct and scattered solar radiation and the proportion of scattered radiation at each tomato leaf level.

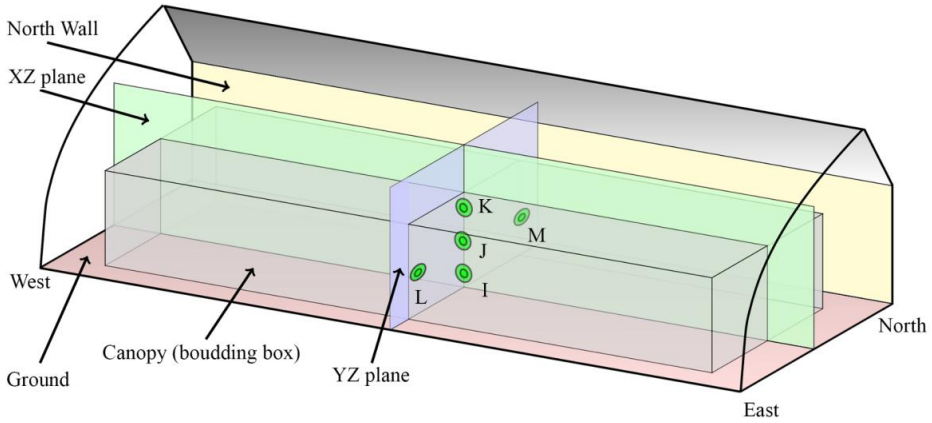

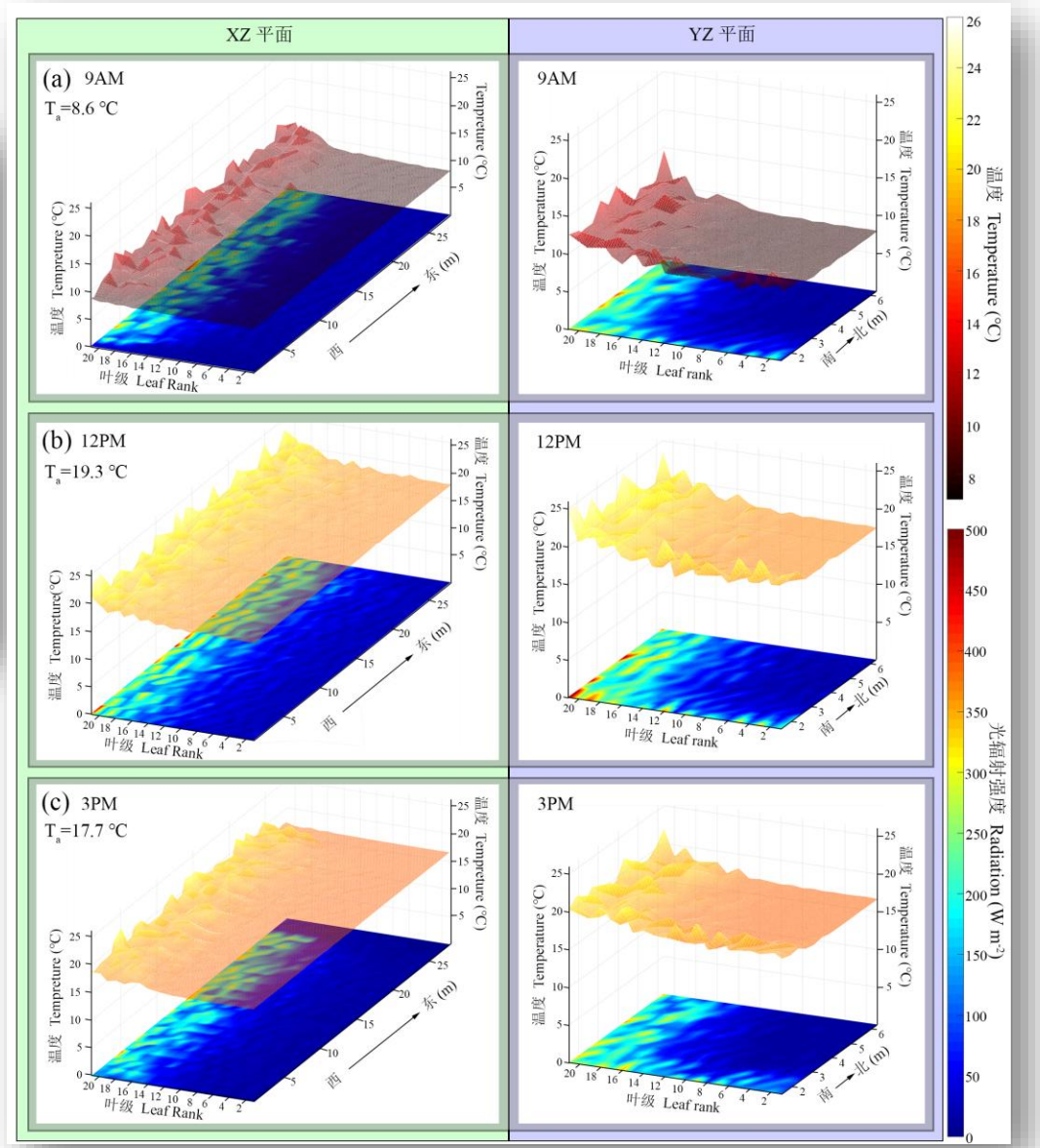

Temperature (the upper 3D diagrams in each sub-figure) and light radiation distribution maps (the lower heat maps in each sub-figure) at 9:00 am (a), 12:00 noon (b), and 3:00 pm (c) on the XZ cross-section and YZ cross-section of the greenhouse canopy.

Contents

Simulation of the Distribution of Photosynthetic Rate of Tomato Leaves in Solar Greenhouses

The Distribution of Photosynthetic Rate of Tomato Population in ESG at 12:00 noon on a Sunny Day.

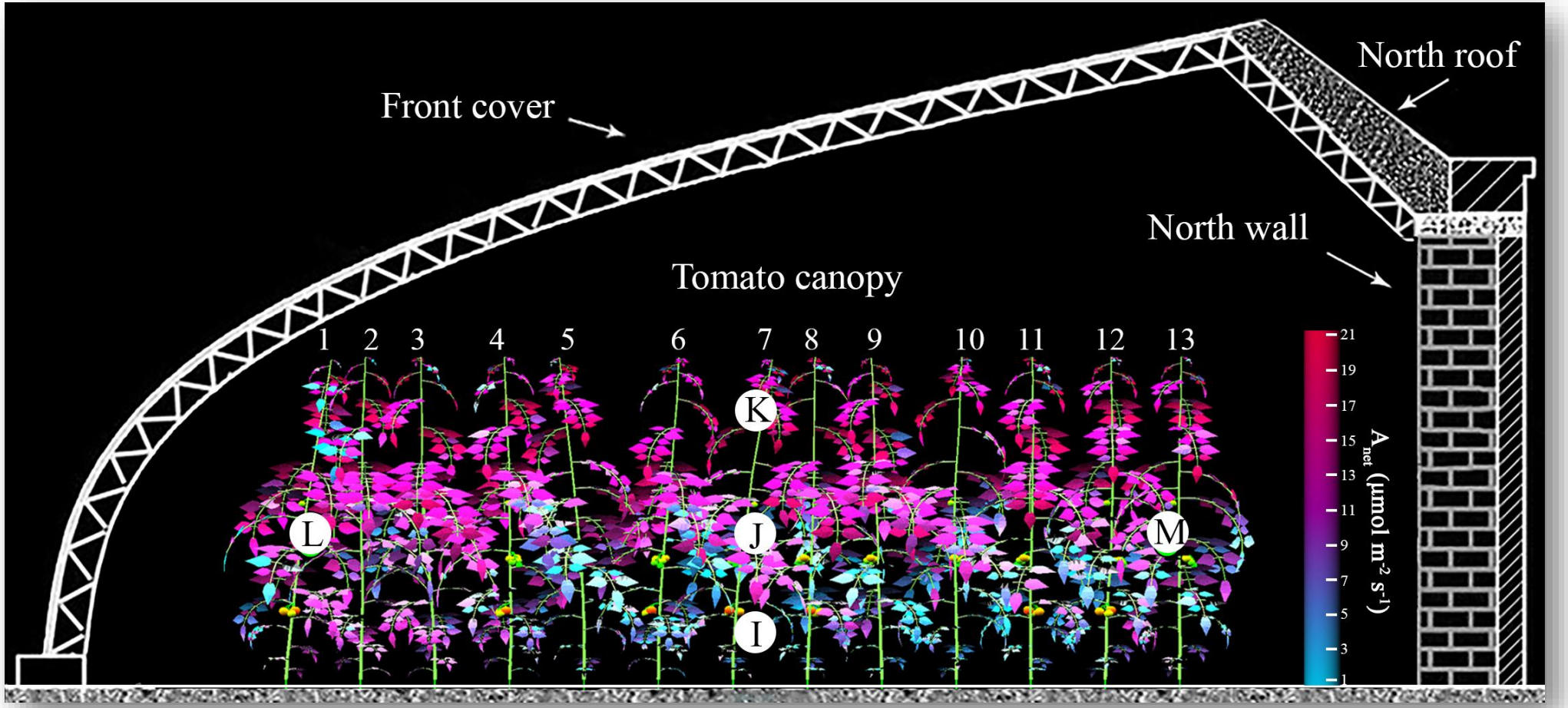

Simulated cloud map of the distribution of leaf photosynthetic rate of a single row of tomatoes in the center of LSG at 12:00 noon; Photosynthetic measurement points (I - M --- Leaf level = 4, 12, 20, 12, 12)

5.2 Simulation Analysis of Photosynthetic Rate

Simulation Analysis of Photosynthetic Rate of Tomato Leaves in Solar Greenhouses

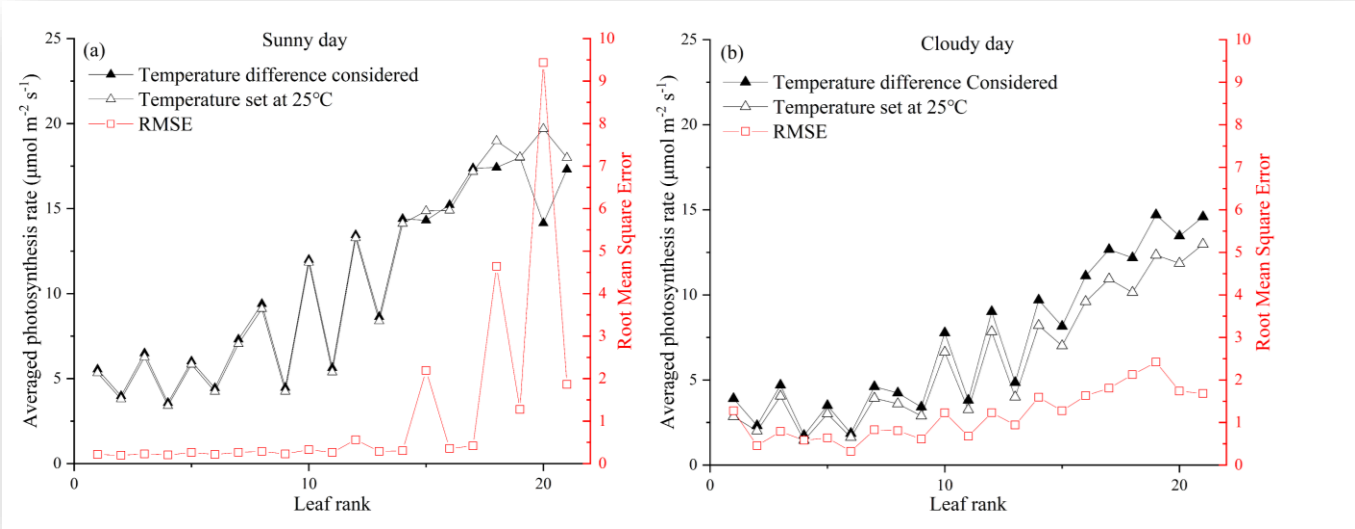

Comparison of the differences in methods between considering leaf temperature variations and setting a constant leaf temperature of 25 ℃ for a single tomato plant at the center of the greenhouse at noon on sunny days (a) and cloudy days (b).

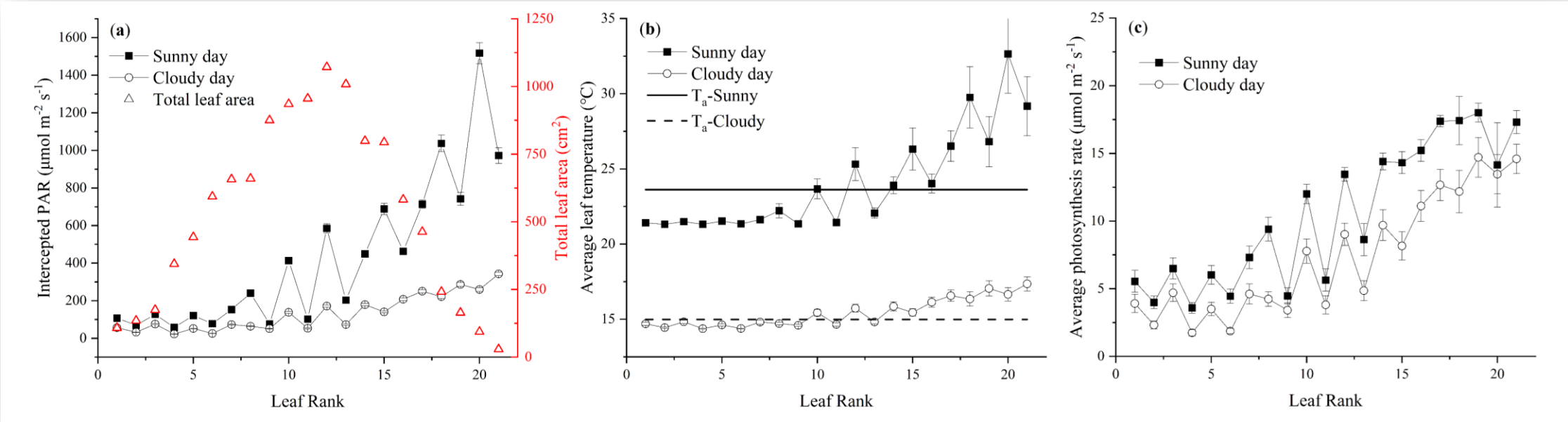

The amount of light intercepted by each leaf layer of a single plant in the middle of the greenhouse at 12:00 noon under sunny and cloudy conditions (a); The average leaf temperature (b); The average net photosynthesis (c) .

5.3 Simulation Analysis of Photosynthetic Limiting Factors

Simulation Analysis of Limiting Factors for the Photosynthetic Rate of Tomato Leaves in Solar Greenhouses

The four main limiting factors of the photosynthetic rate of tomato leaves inside solar greenhouses on sunny and cloudy days: stomatal conductance limitation (SL), mesophyll conductance limitation (ML), biochemical capacity limitation (BL), and light limitation (LL).

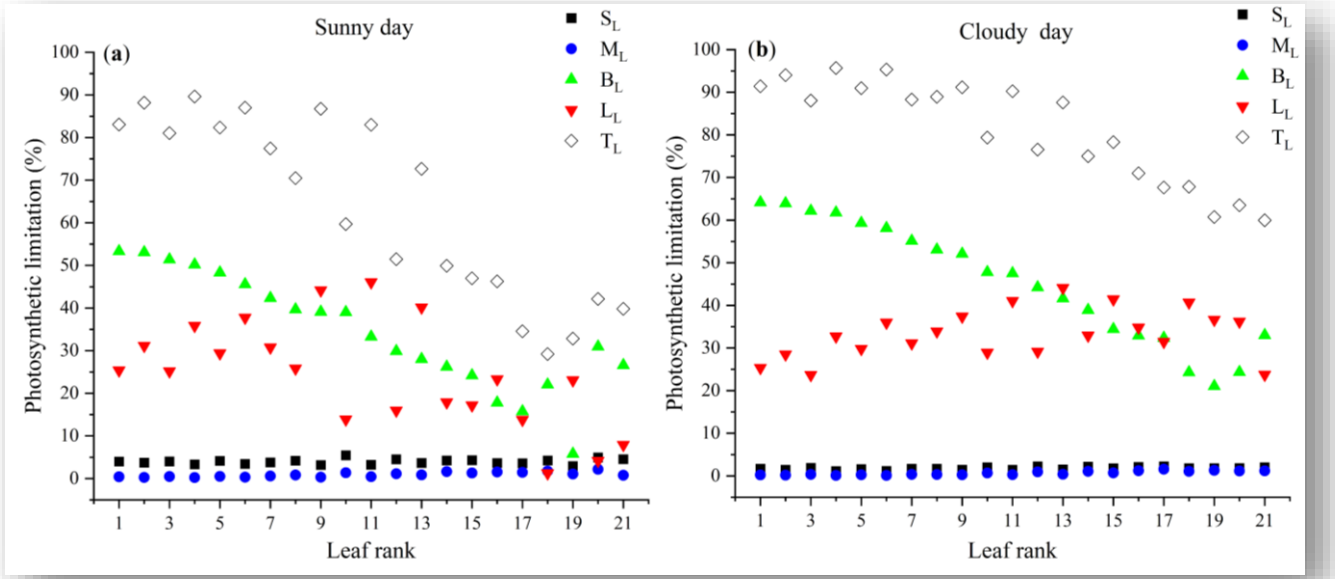

Comparison of the percentages of each photosynthetic limiting factor at each tomato leaf level at 12:00 noon on sunny and cloudy days.

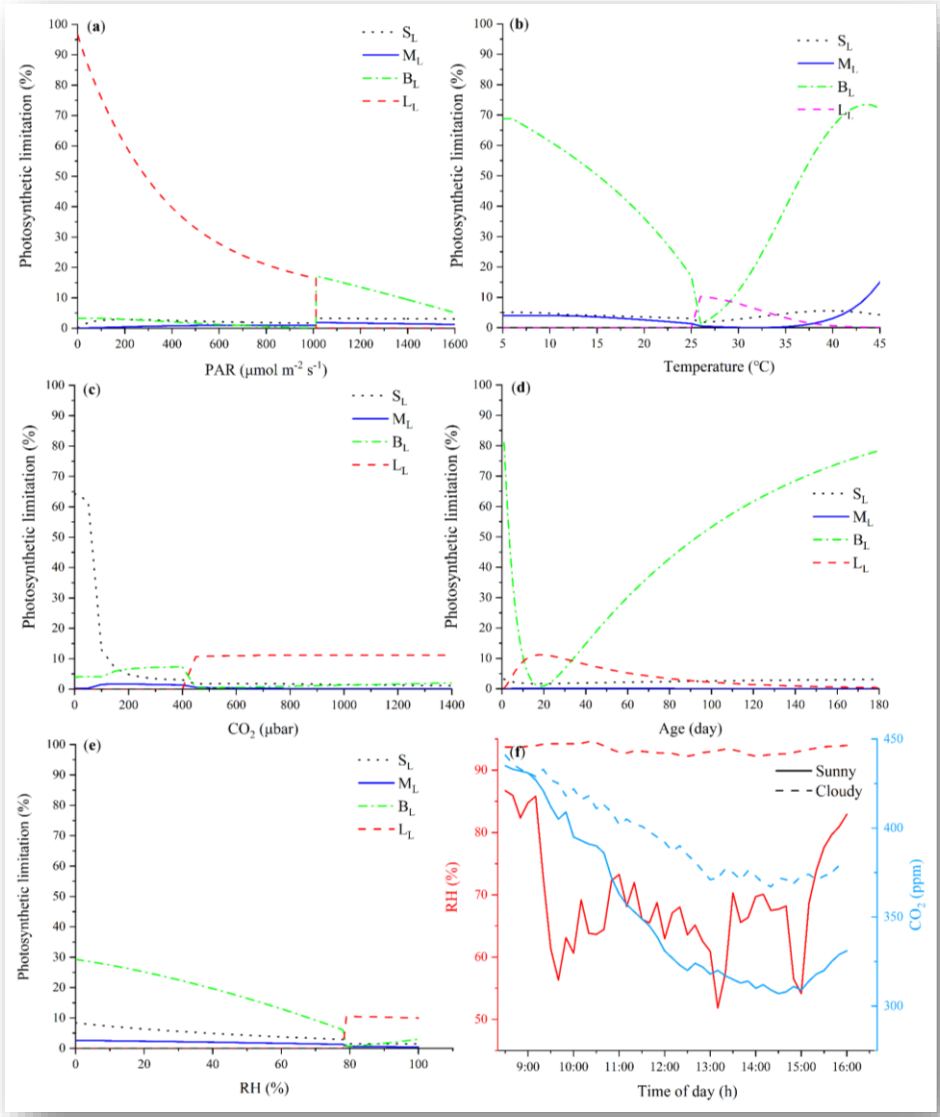

Performance of each photosynthetic limiting factor under different condition changes: PAR (μmol m^{-2} s^{-1}) (a), leaf temperature (°C) (b), CO_2 concentration (μbar) (c), leaf age (number of days after unfolding) (d), RH (%) (e), and the daily measured RH and CO_2 concentration in the greenhouse on sunny and cloudy days (f).

Contents

6.1 Simulation of Tomato Plant Configuration in Solar Greenhouses

Simulation of Tomato Planting Configuration:

The greenhouse tomato planting is divided into the following two ridge directions:

- North-south ridges
- East-west ridges

Four planting patterns:

- Even planting
- wide-narrow rows
- staggered rows
- incremental rows

Sixteen densities:

- Furrow distance: 1-1.6 m
- Plant spacing: 0.3-0.6 m

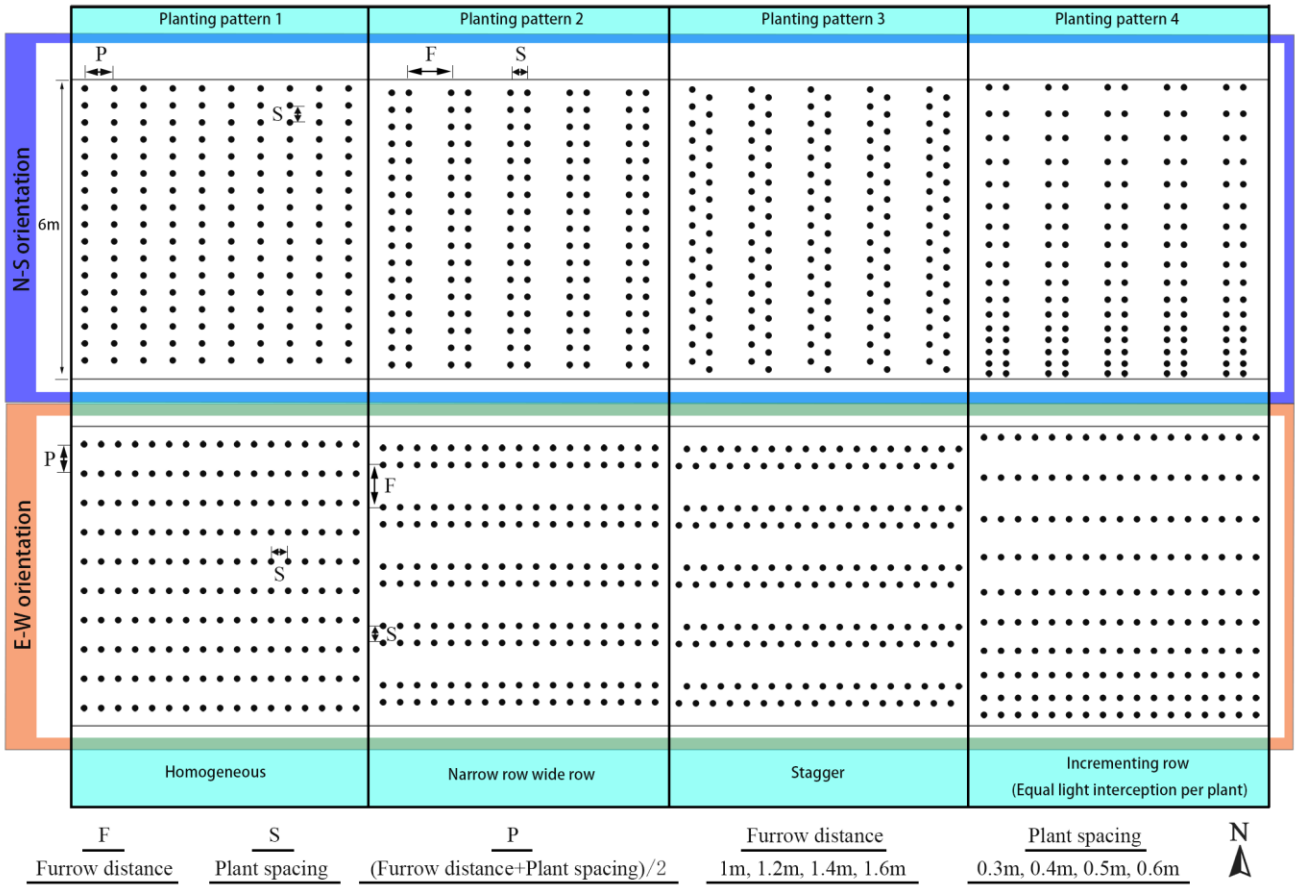

Schematic diagrams of four planting patterns in the NS row direction (a) and the EW row direction (b), namely: even planting (planting pattern 1), wide-narrow rows (planting pattern 2), staggered rows (planting pattern 3), and incremental rows (planting pattern 4).

6.1 Simulation of Tomato Plant Configuration in Solar Greenhouses

Comparison of Different Plant Configurations:

Taking the most common ridge spacing of 1 m and plant spacing of 0.3 m as examples, the noon light interception situation of a single plant for the following 8 plant configurations was simulated:

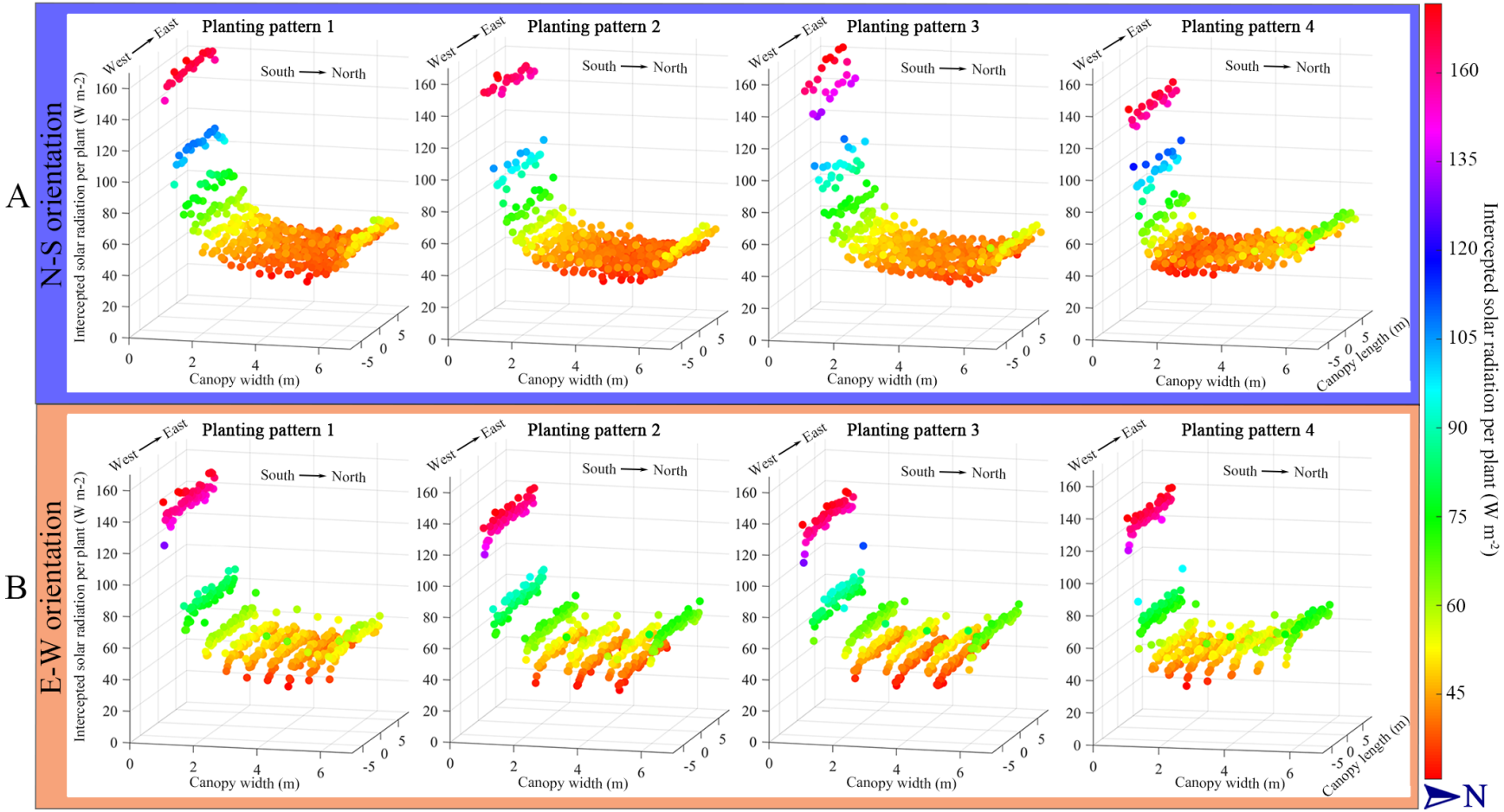

The amount of solar radiation intercepted by a single plant at noon under four planting patterns in the north-south direction (above) and the east-west direction (below). Each sphere, height, and color represent the intensity of the solar radiation intercepted by the whole plant, which is the sum of the absorbed radiation by all the leaves and leaflets of the plant.

6.1 Simulation of Tomato Plant Configuration in Solar Greenhouses

Comparison of light interception amount (a, b), leaf temperature (c, d), and photosynthesis (e, f) among the two ridge directions and four planting patterns as the plant spacing and ridge spacing increase.

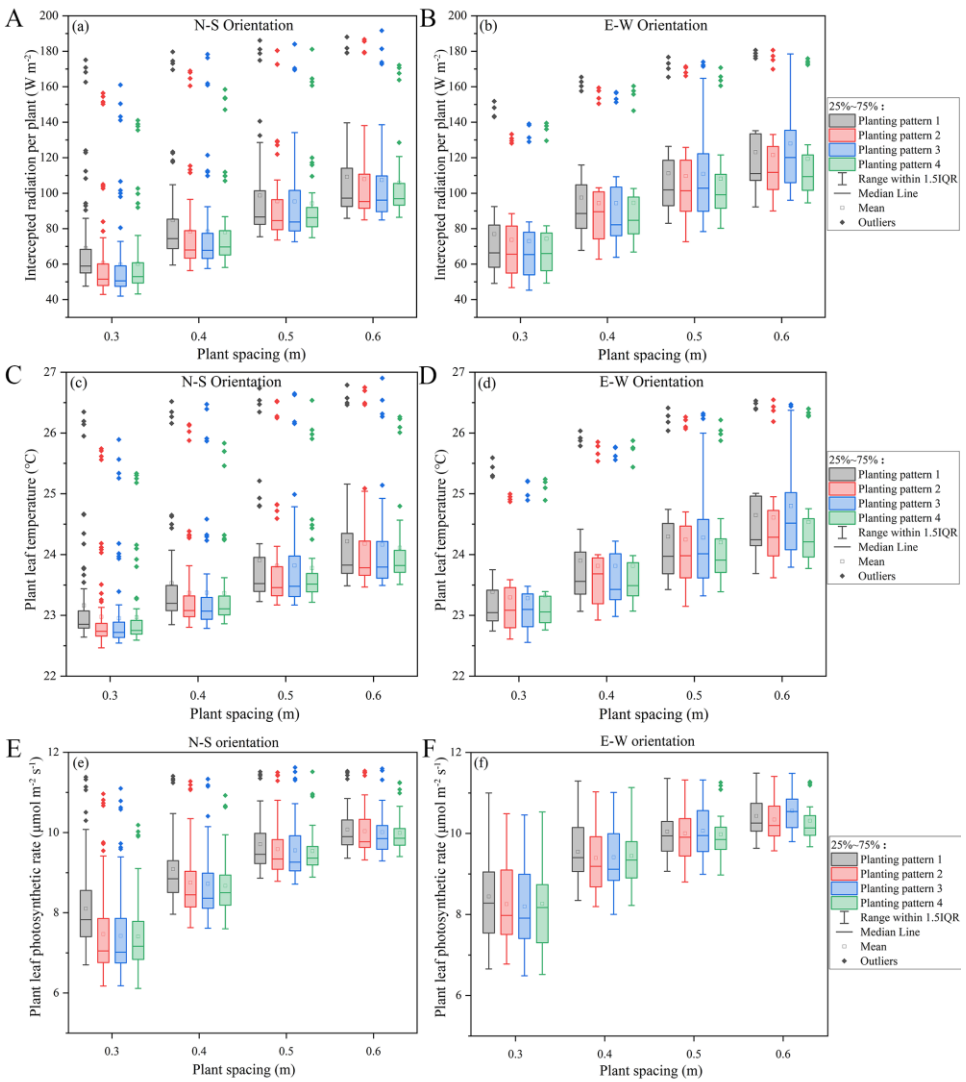

With the increase in plant spacing, the noon solar radiation interception amount (a, b), leaf temperature (c, d), and photosynthesis (e, f) of the four planting patterns in the NS direction (a, c, e) and the EW direction (b, d, f).

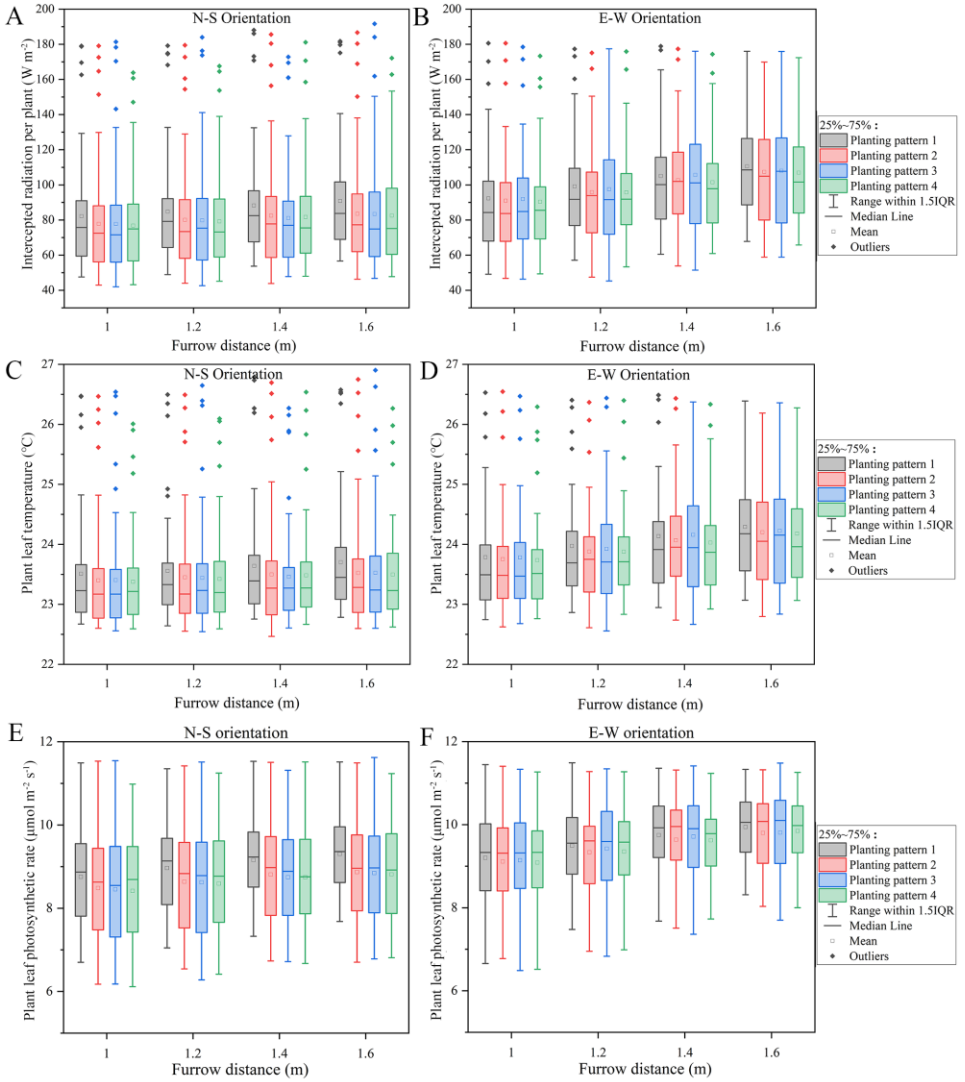

With the increase in ridge spacing, the noon solar radiation interception amount (a, b), leaf temperature (c, d), and photosynthesis (e, f) of the four planting patterns in the NS direction (a, c, e) and the EW direction (b, d, f).

6.1 Simulation of Tomato Plant Configuration in Solar Greenhouses

Comparison of Different Plant Configurations:

Detailed comparison of three points of plants (A, B, C) between the north-south ridge direction and the east-west ridge direction in planting pattern 4 (incremental rows).

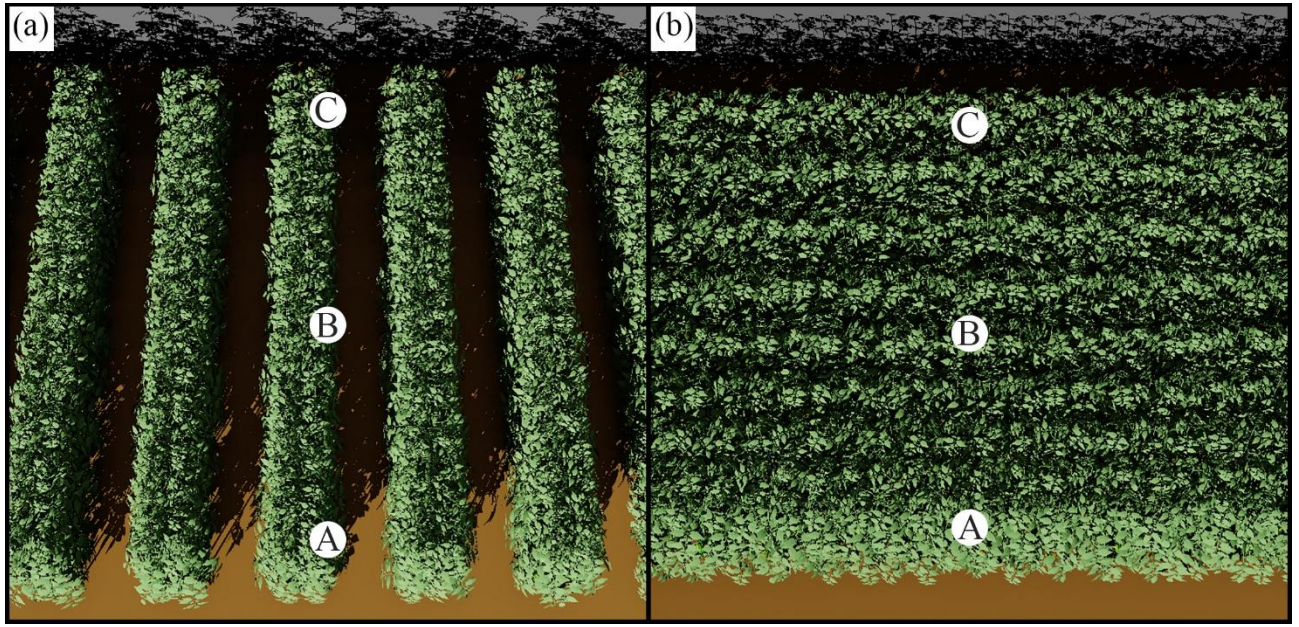

With the increase in plant spacing, the noon solar radiation interception amount (a, b), leaf temperature (c, d), and photosynthesis (e, f) of the four planting patterns in the NS direction (a, c, e) and the EW direction (b, d, f).

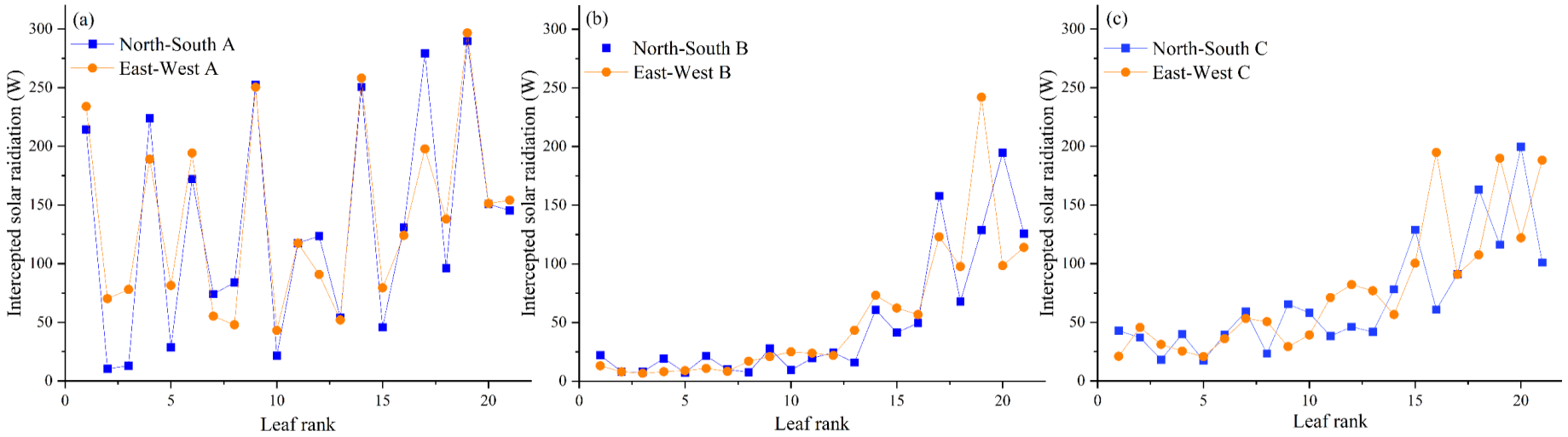

With the increase in ridge spacing, the noon solar radiation interception amount (a, b), leaf temperature (c, d), and photosynthesis (e, f) of the four planting patterns in the NS direction (a, c, e) and the EW direction (b, d, f).

Comparison of Different Plant Configurations

Conduct a comparison of light radiation at three leaf levels (4, 11, 18) in different time periods (9 a.m., 12 p.m., 4 p.m.) between the north-south ridge direction and the east-west ridge direction in planting pattern 4 (incremental rows).

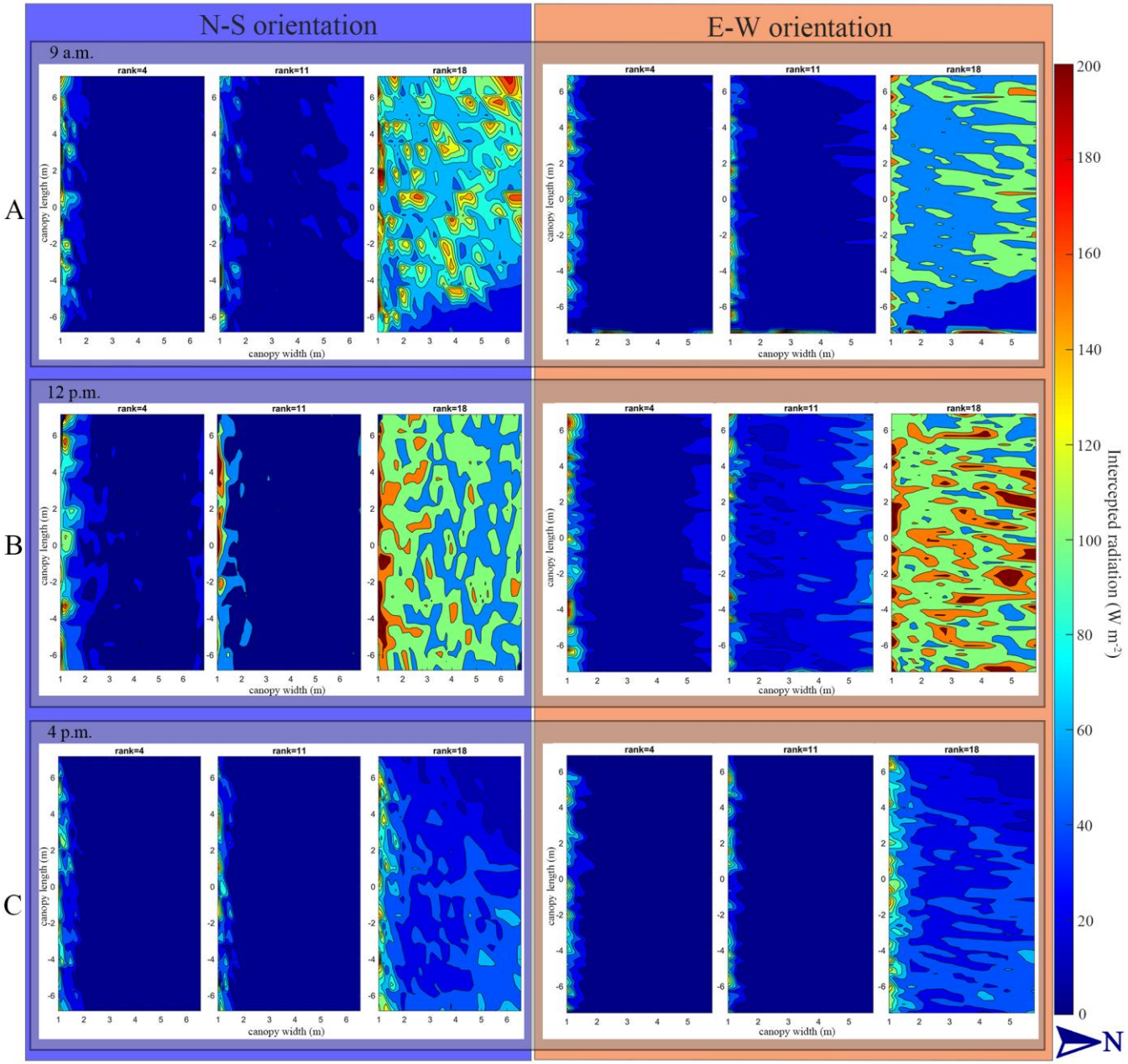

6.2 Simulation of Tomato Plant Architecture in Solar Greenhouses

Simulation of Different Plant Architecture Structures of Tomato：

8 configurations: 4 at the branch level; 4 at the leaf level. The total leaf area of a single plant remained unchanged for each treatment.

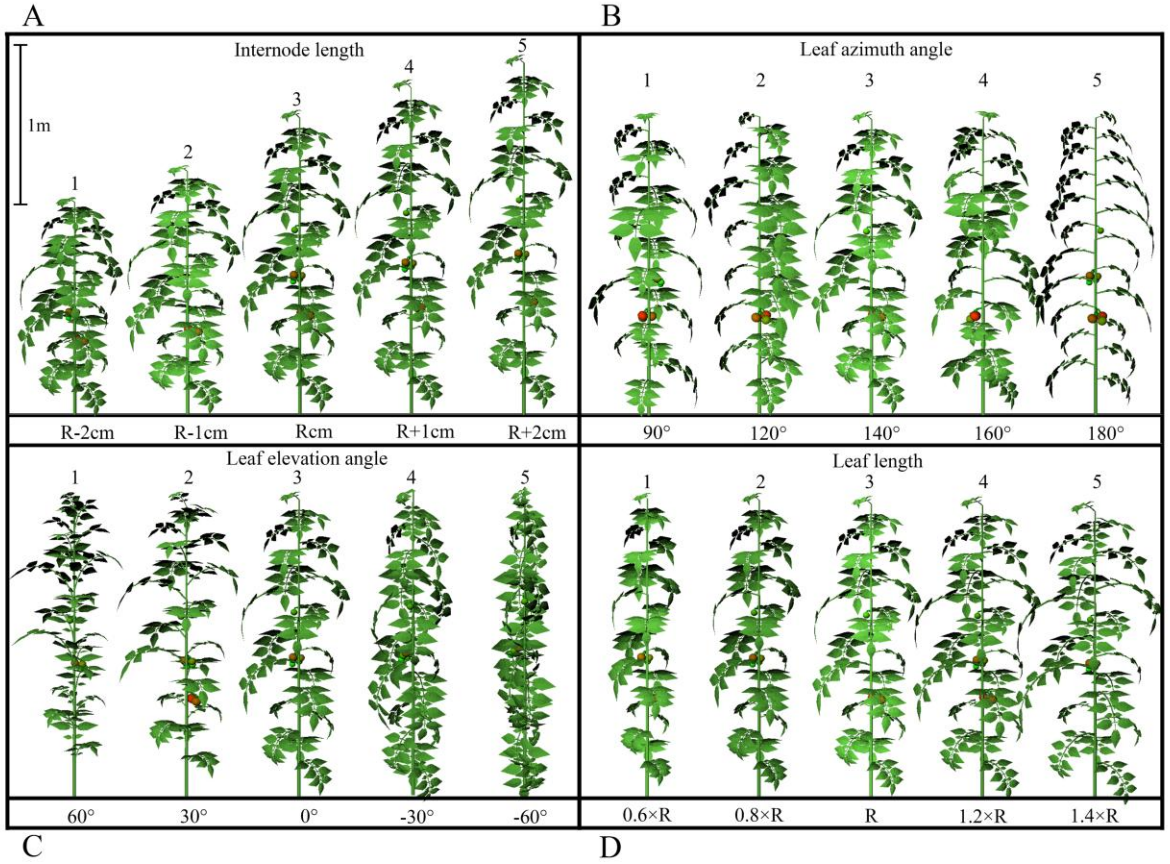

Detailed simulation configurations of the characteristics at the tomato branch level. Each tomato plant was simulated individually, and there were 5 treatments in each scenario. For each leaf level of the tomato plant in each treatment, there was a corresponding visual 3D representation, namely: internode length (R - 2 cm, R - 1 cm, R cm, R + 1 cm, R + 2 cm), branch azimuth angle (90°, 120°, 140°, 160°, 180°), branch elevation angle (60°, 30°, 0°, -30°, -60°), and branch length (0.6 × R, 0.8 × R, R, 1.2 × R, 1.6 × R).

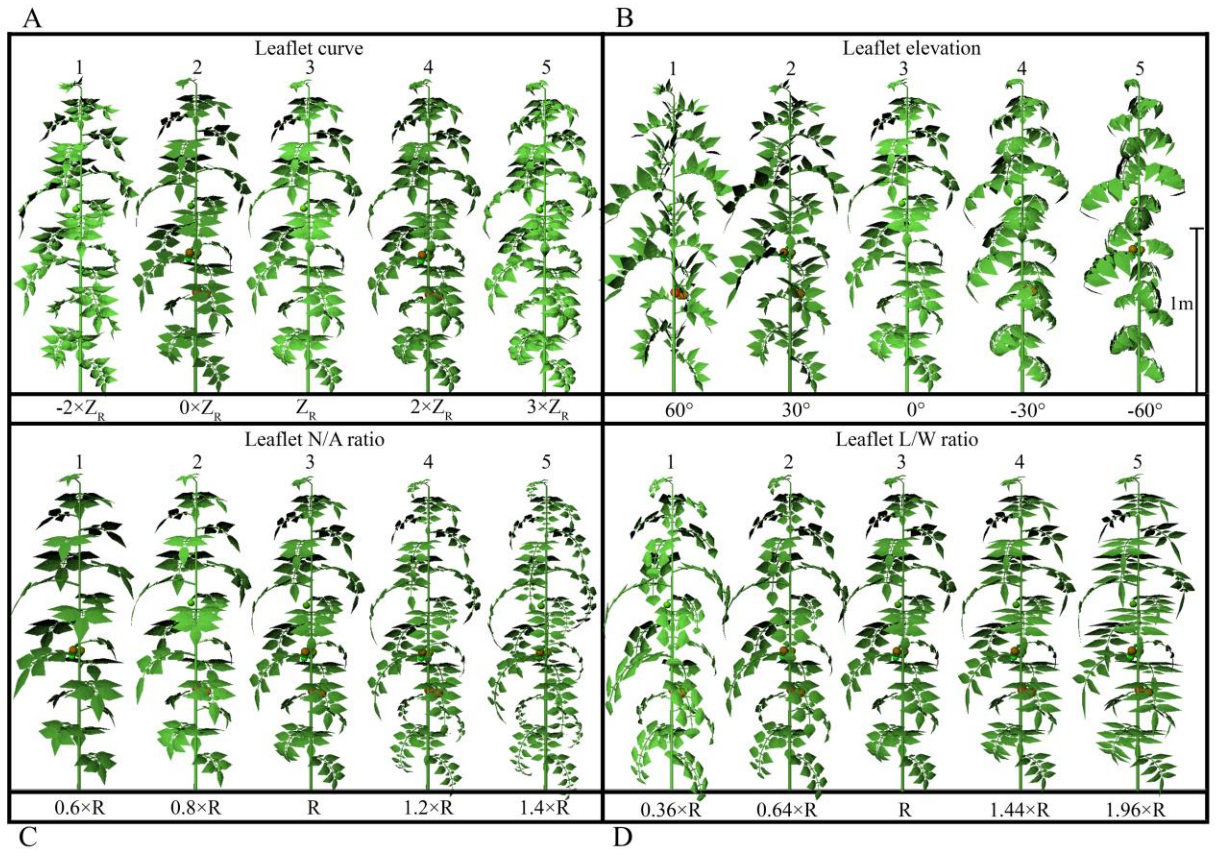

Detailed simulation configurations of the characteristics at the tomato leaf level. Each tomato plant was simulated individually, and there were 5 treatments in each scenario. For each leaf level of the tomato plant in each treatment, there was a corresponding visual 3D representation, namely: leaf curvature (-2×ZR, 0×ZR cm, ZR cm, 2×ZR, 3×ZR), leaf elevation angle (60°, 30°, 0°, -30°, -60°), leaf number/area (0.6×R, 0.8×R, R, 1.2×R, 1.4×R), and leaf width/length ratio (0.36×R, 0.64×R, R, 1.44×R, 1.96×R). LR represents the reference value of leaf length. ZR is the reference value of the ordinate of leaf curvature.

6.2 Simulation of Tomato Plant Architecture in Solar Greenhouses

Comparison of Light Interception and Accumulation at the Leaf Level among Different Plant Types：

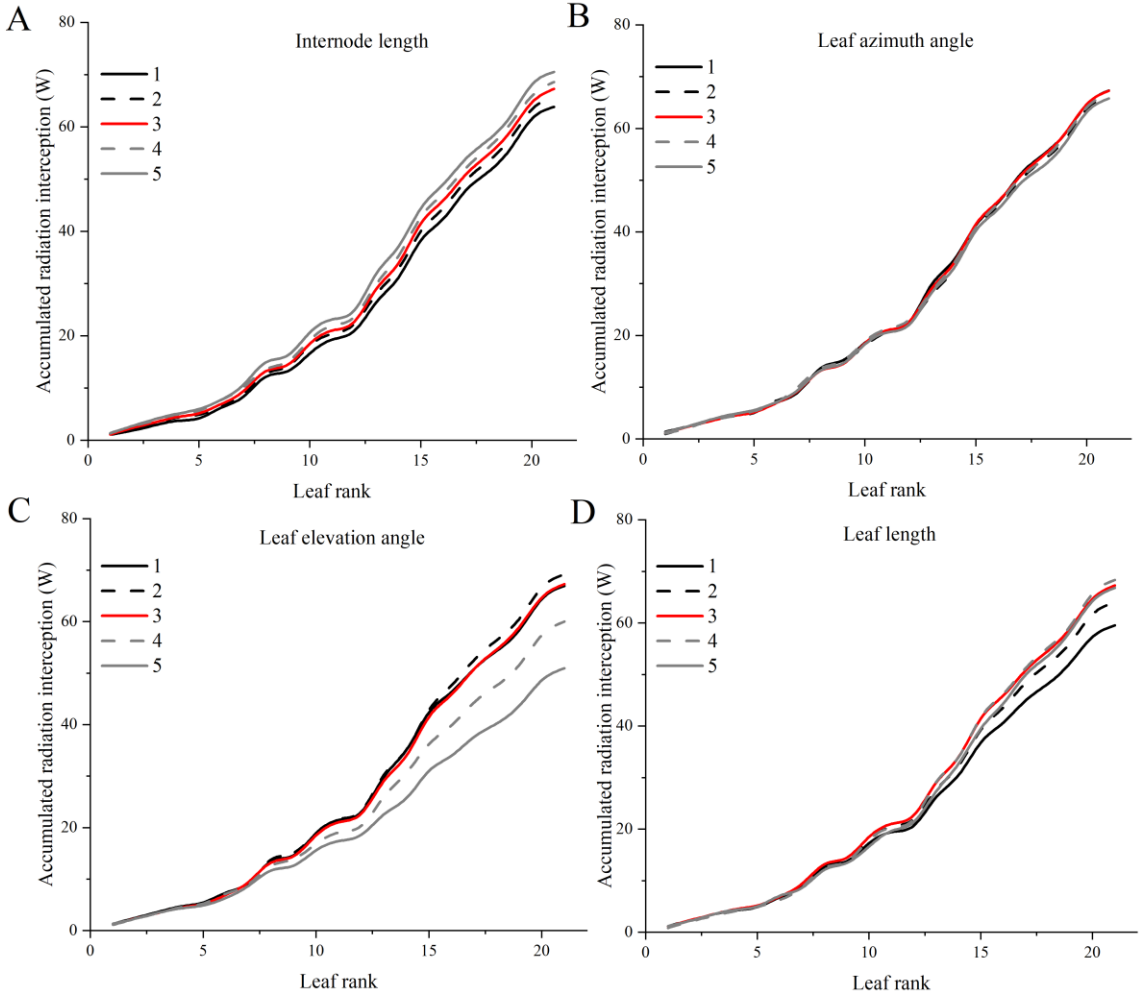

The effects of different treatments of branch horizontal shapes on the cumulative light radiation per plant with the increase of leaf grade. A single plant located in the center of the greenhouse was simulated to avoid any boundary effects. For example, internode length (a), leaf azimuth (b), leaf elevation angle (c), and leaf length (d).

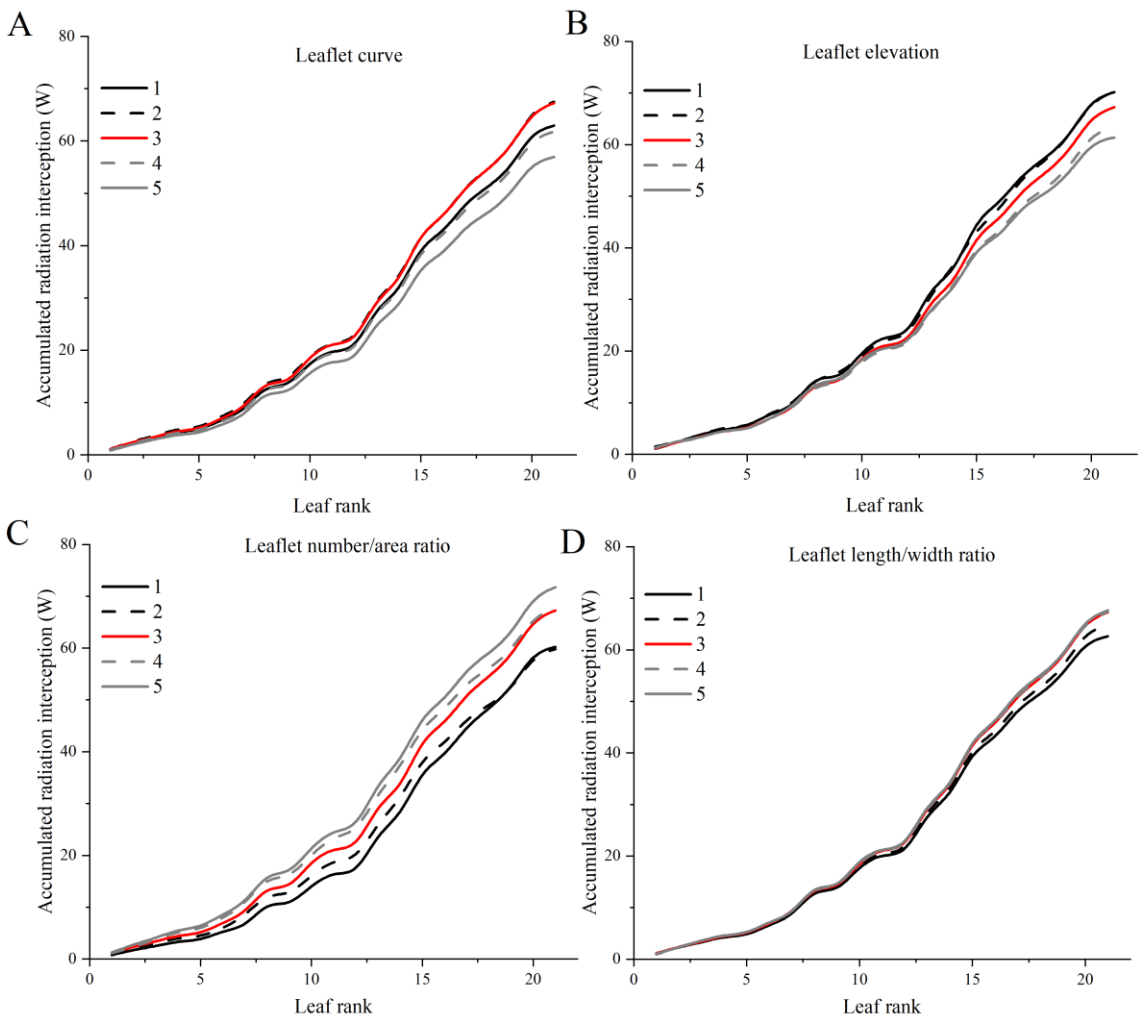

The effects of different treatments of leaf horizontal shapes on the cumulative light radiation per plant with the increase of leaf level. A single plant located in the center of the greenhouse was simulated. For example, leaflet area (a), leaflet height (b), leaflet number (c), and leaflet width-to-length ratio (d).

6.2 Simulation of Tomato Plant Architecture in Solar Greenhouses

The comparison between photosynthetic rate and dry matter of different plant types:

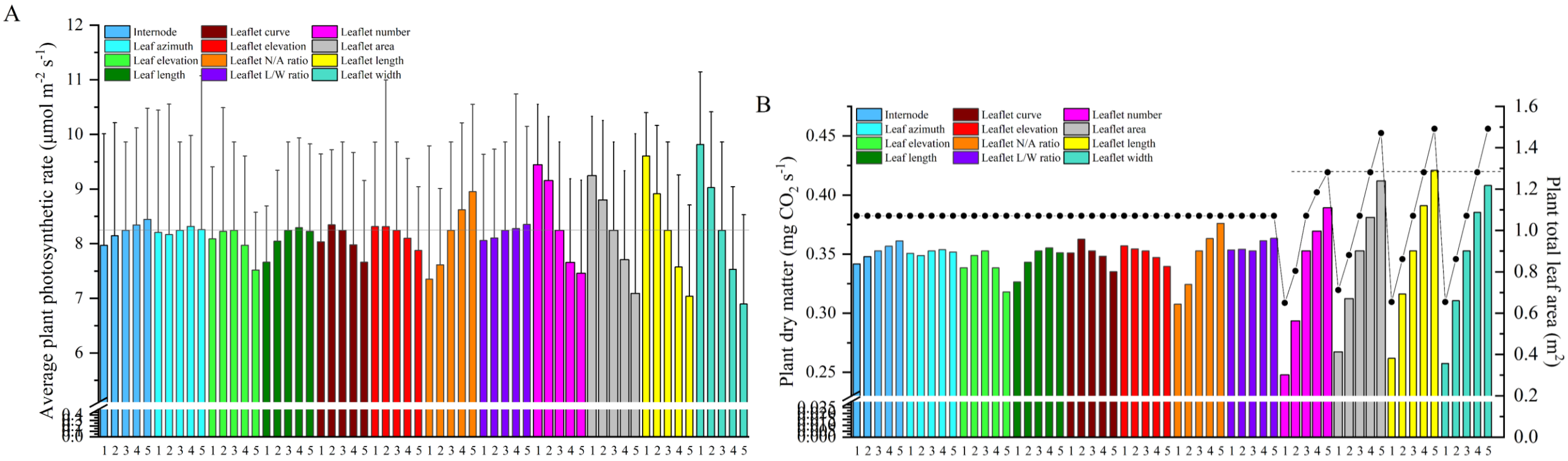

The effects of different plant type treatments on the average photosynthetic rate (a) and the amount of dry matter accumulation per plant (b).

6.2 Simulation of Tomato Plant Architecture in Solar Greenhouses

Comparison between the ideal plant architecture and the measured reference plant architecture.

The light radiation interception capacity of the canopy has been increased by 20.21%.

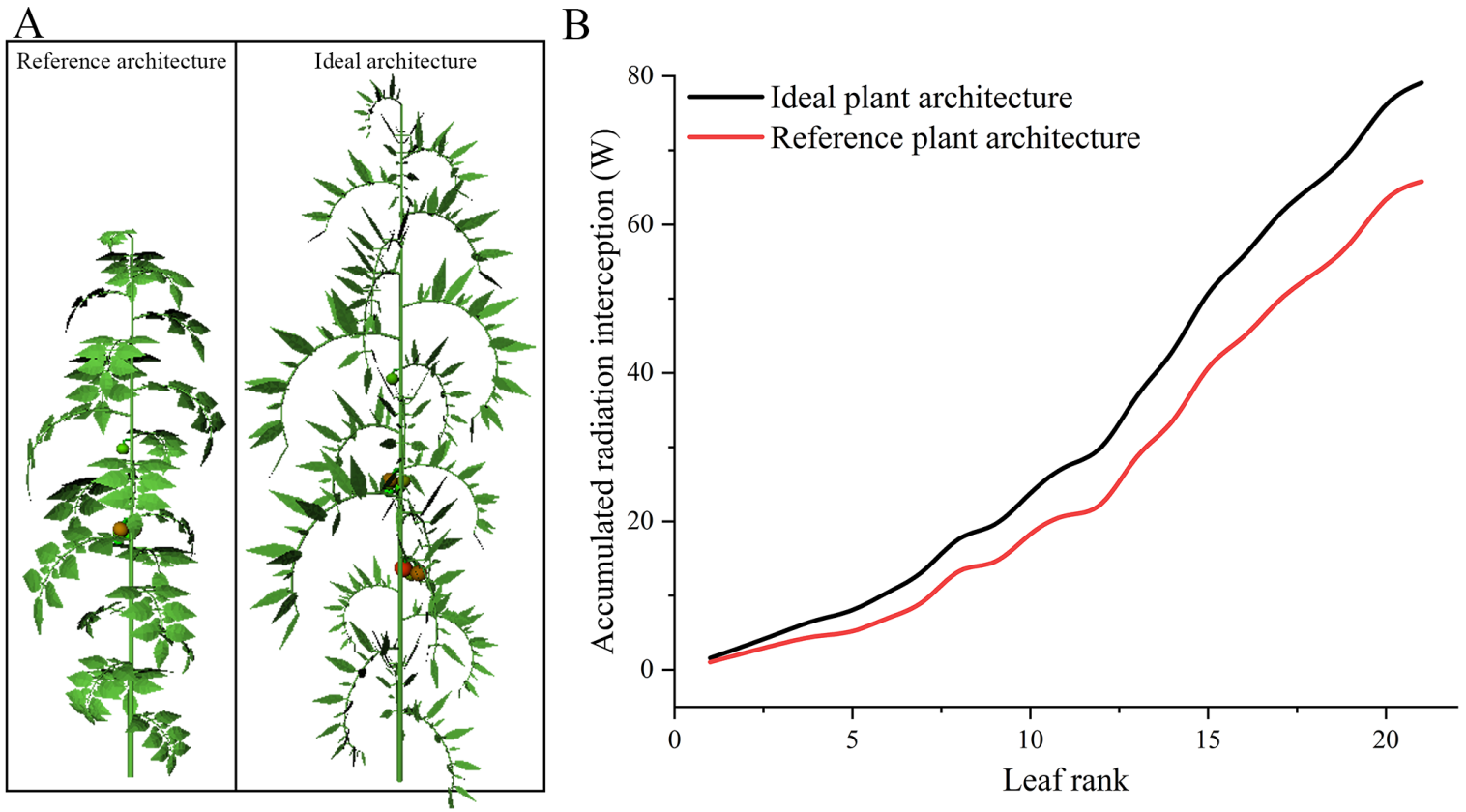

	Internode length	Leaf azimuth angle	Leaf elevation angle	Leaf length	Leaflet curve	Leaflet elevation	Leaflet N/A ratio	Leaflet L/W ratio
Reference	R	140 °	0 °	R	R_z	0 °	R	R
Ideal	R+2 cm	160 °	0 °	1.2×R	0	60 °	1.4×R	1.96×R

Comparison between the original reference tomato plant type structure and the ideal tomato plant type structure obtained by integrating the optimal values of various plant type parameters derived from simulation screening.

Partial Least Squares Path Modeling:

Partial Least Squares Path Modeling (PLS-PM) is a structural equation modeling (SEM) technique. It is mainly used to analyze the complex causal relationships among multiple variables, especially in the presence of latent variables. Theoretically speaking, it can be applied to purely simulated data.

We thus performed PLS-PM on all the simulated physiological and morphological data to explore the causal and quantitative relationships among variables.

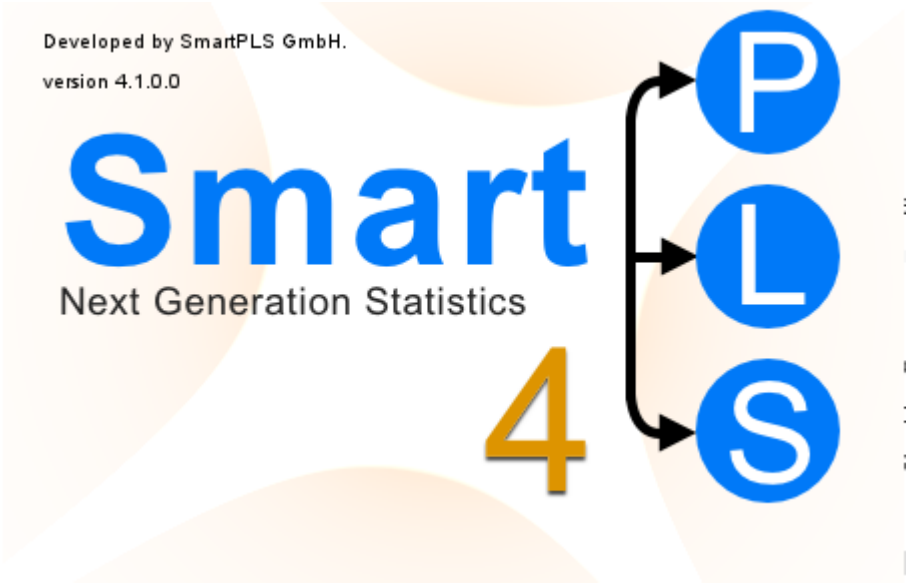

6.2 Simulation of Tomato Plant Architecture in Solar Greenhouses

Partial Least Squares Path Modeling:

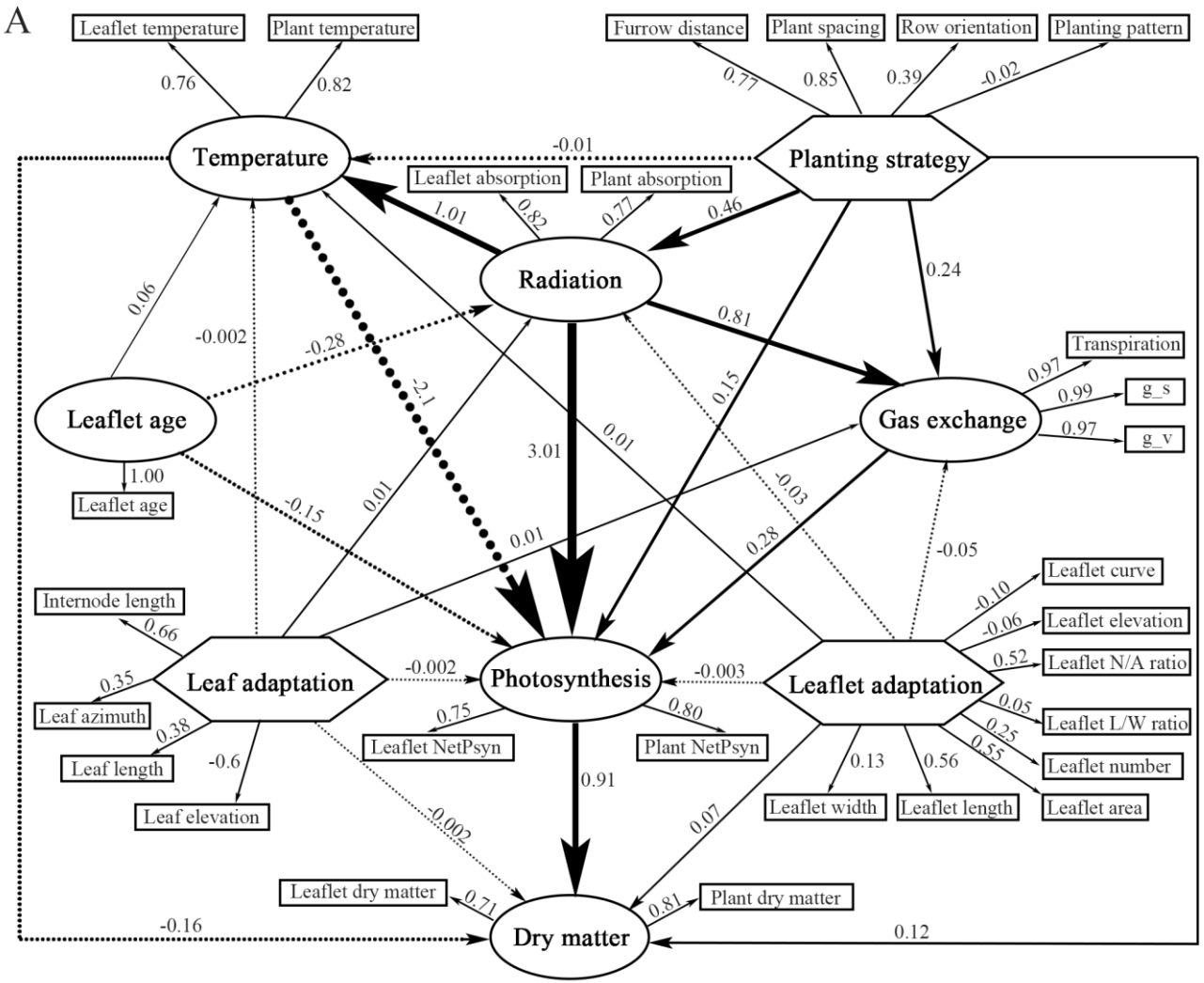

Partial Least Squares Path Modeling (PLS-PM) of all the simulated physiological and morphological data. The simulated variables are represented in rectangular form, while the characteristics within the large circles and polygons are latent variables (LV). The numbers above indicate the loadings (the correlations between the latent variables and their simulated variables) and the path coefficients calculated after 1,000 bootstraps.

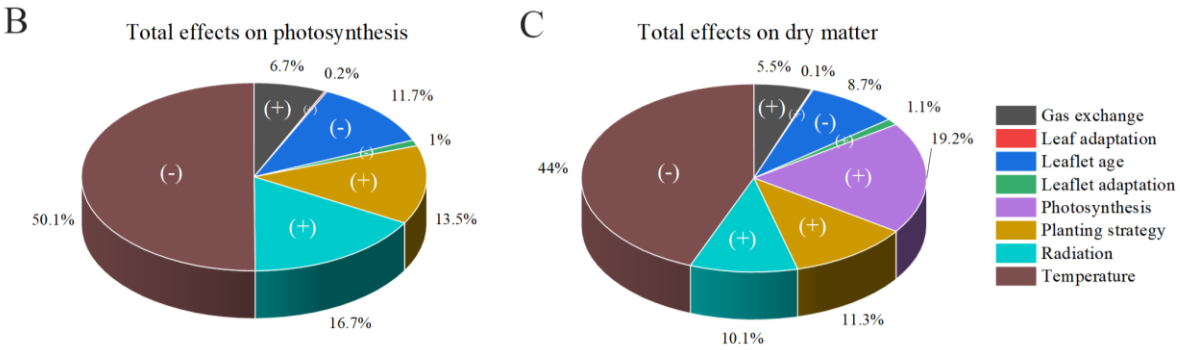

The total effects of different LV on the PLS-PM output: photosynthesis and yield. (+) indicates a positive impact, while (-) indicates a negative impact. The percentages are the proportions of the path weights that contribute to each output.

Contents

Summary

The following achievements have been made:

1. Optimization of the Structure of the Second-generation ESG in China

2. Simulation of Environmental Factors and Photosynthetic Rate at the Leaf Level of Tomatoes in ESG

3. Comparative Analysis of Canopy Structure Scenarios for Different Planting Configurations

Thanks!